The influence of innovative photovoltaic technologies on urban energy systems

An energy system analysis with concentrator PV, perovskite-silicon PV and PV-powered heat pumps in comparison with state-of-the-art technologies

Working Paper

July 22, 2021

Imprint

Carried out by:

Reiner Lemoine Institut
www.reiner-lemoine-institut.de
info@rl-institut.de
Rudower Chaussee 12
12489 Berlin

Authors:

Sabine Haas, Inia Steinbach, Marie-Claire Gering, Caroline Möller

Acknowledgements:

This project has received funds from the European Union's Horizon2020 research and innovation programme under Grant Agreement 787289.

Abstract

Cities need to make a contribution in reducing greenhouse gas emissions if the climate goals of the Paris Agreement and the resulting national and regional targets are to be achieved. The space for renewable energy in urban areas, however, is limited, while the demand per area is comparatively high, as there is a tendency for multi-storey buildings. To reduce the urban dependence on rural areas associated with the energy system transformation towards decarbonisation, the ratio between generation and demand in cities should be improved. The scientific community is developing highly efficient photovoltaic technologies that may be a solution to the space limitation for renewable energy in cities, while heat pumps are explored as a way to decarbonise the heat sector. In this study, we have analysed the effects of three innovative photovoltaic technologies on urban residential energy systems: a hybrid high concentrator photovoltaic silicon module, a fictitious high efficient tandem perovskite silicon module, and a photovoltaics-powered heat pump. We have examined the effect on the degree of autonomy, self-consumption, total system costs, and greenhouse gas emissions of the energy system in comparison to standard multi-crystalline silicon photovoltaics and fossil heat supply from a gas boiler in an energy system analysis with linear optimisation. Additionally, we have explored the potential for supplying net zero energy communities with these technologies. We have focused on the local energy system of fictitious residential areas of 20 buildings under two different climatic conditions in Madrid (Spain) and Berlin (Germany). As especially concentrator photovoltaics are highly dependent on the direct irradiance, we have examined the influence of the location in ten additional European locations. We have found that under current regulations, specific investment costs of concentrator photovoltaics and perovskite-silicon would have to be lowered in order to compete with silicon technology. However, the use case of net zero energy communities shows the advantage of the space saving technology of concentrator photovoltaics. For perovskite-silicon, as a technology positioned between concentrator photovoltaics and silicon in terms of efficiency and specific investment costs, we found no plausible advantage over silicon in the calculated scenarios. However, due to its low technological readiness level, our assumptions for perovskite-silicon technology are more uncertain compared to the other technologies. We have further demonstrated that photovoltaics-powered heat pumps are an appropriate technology for increasing the self-consumption and lowering the greenhouse gas emissions of an energy system.

Contents

Acronyms

AOI angle of incidence

BDEW Bundesverband der Energie- und Wasserwirtschaft

BOS balance of system

CdTe cadmium tellurium

CIS Cadmium Indium Selenide

COP coefficient of performance

COP21 Paris climate conference

CPV concentrator photovoltaics

CPV/T concentrating photovoltaics/thermal

CRF capital recovery factor

DA degree of autonomy

DHI diffuse horizontal irradiance

DNI direct normal irradiance

EU European Union

EQE external quantum efficiency

GHG greenhouse gas

GHI global horizontal irradiance

HCPV high concentrator photovoltaics

HP heat pump

KPI key performance indicator

LCOE levelised costs of electricity

MSP minimum sustainable price

MVS Multi-Vector Simulator

NPEB net-positive energy building

NZE net zero energy

nZEB nearly zero energy building

NZEB net zero energy building

OM operation and maintenance

PR performance ratio

PSI perovskite-silicon

PV photovoltaics

PV photovoltaic

SC self-consumption

SI silicon

SMARTS Simple Model of the Atmospheric Radiative Transfer of Sunshine

TES thermal energy storage

TRL technological readiness level

1. Introduction

Limiting global warming below 2°C, preferably to 1.5°C, compared to the pre-industrial average temperature, was agreed on in the Paris Agreement, which was signed by more than 190 countries at the Paris Climate Conference (COP21) in 2015. Targets for greenhouse gas (GHG) emission reductions and the share of renewables in energy supply exist on European, national, and regional levels. In order to reach them, all stakeholders on governmental and non-governmental level, such as municipalities and cities, the civil society, businesses, etc. are urged to contribute to reaching these goals (on Climate Change (UNFCCC), 2016; Tollin, 2016). Concerning the implementation, urban areas are dependent on rural areas, as urban areas have a disadvantageous ratio of renewable energy generation potential and energy demand due to a higher population density. Thus, in a future decarbonised energy system with space-intensive renewable energy plants, urban areas might depend even more on rural areas than today, where part of the demand is covered by less space-intensive fossil power plants (Möller, Faulstich, & Rosenberger, 2019). In cities, the space that is available for renewable energy is limited. As there is scarcely space for large wind energy converters or ground-mounted photovoltaics (PV), buildings are the main location for renewable energy converters. The most common technology for buildings is rooftop PV and – also promising – PV on facades and building-integrated PV. Most of the buildings in cities belong to the residential sector and it is, therefore, necessary to motivate the building owners' participation, e.g. by financial incentives. High local renewable energy contribution could be reached by incentives that reward high degrees of autonomy (DA) and net zero energy buildings (NZEBs), while high self-consumption (SC) is already rewarded in places where the feed-in tariff is lower than the electricity price (Beck, Kondziella, Huard, & Bruckner, 2017a).

The European Union (EU) reacted with an additional directive recast that requires all new buildings in the EU to be nearly zero energy buildings (nZEBs) since the end of 2020 (Directive 2010/31/EU) (Parliament & Council, 2010). The directive defines nZEBs as buildings with a very low energy demand which "should be covered to a very significant extent by energy from renewable sources, including energy from renewable sources produced on-site or nearby" (see Parliament & Council, 2010). While this concept of nZEBs does not clearly state to which extent energy should be generated on-site, the concept of NZEBs goes further and requires the demand to be fully covered by energy generated on-site on an annual balance. This means, energy consumed from the grid should not exceed the energy that is fed into the grid during the period of one year (Cole & Fedoruk, 2015; Voss, Musall, Sartori, & Lollini, 2013). However, definitions of NZEBs in literature are diverse; see e.g. (Cole & Fedoruk, 2015) that lists literature on definitions of NZEBs and further examines the definitions of nZEBs and net-positive energy buildings (NPEBs), with the latter providing more renewable energy than they consume.

We define NZEBs as buildings which fully meet or exceed their demand from locally generated renewable energy on an annual balance while energy can be exchanged with the grid. Further, we focus on residential net zero energy (NZE) communities, where the system boundaries are extended to include all buildings within one community or neigborhood (see e.g. Pless & Torcellini, 2010; Carlisle, Geet, & Pless, 2009). In this study, we exclude brownfield sites and green space, as defined by Carlisle et al. (2009), assuming that such spaces are not available for renewables in urban areas.

To strive towards NZEB/nZEB and a high degree of autonomy in urban areas, it is necessary to expand the local renewable generation of buildings. As space is a limiting factor here, innovative highly efficient PV technologies are being developed. With a record of a 26,7 % efficiency (Green et al., 2019) for a single-junction cell, the potential of silicon, with a theoretical maximum efficiency of around 30 % (Shockley & Queisser, 1961; Schäfer & Brendel, 2018), is almost fully exploited (Yoshikawa et al., 2017). One way to exceed the 30 % margin is by combining materials with different bandgaps in multi-junction cells.

Within the last decade, research has shown a remarkable rise in the performance of metal halide perovskites solar cells. Especially the combination of a perovskite top cell and silicon bottom cell shows a great potential promising a highly efficient and low-cost solution. The tunable bandgap of perovskites (ca 1.5–2.2 eV) allows for an ideal complement to the low-cost and well established silicon (Sofia et al., 2019). In December 2020, a record of 29.52 % efficiency has been achieved by Oxford PV for perovskite-silicon (PSI) tandem structures (Hutchins, 2020). Perovskite allows for an easy and low-cost fabrication. Due to the high absorption coefficient, the complete visible solar spectrum can be absorbed by ultra thin films which reduces material costs even more (Yin, Shi, & Yan, 2014). Up to now, research has only been limited to laboratory settings, showing that the lifetime of perovskite is still very limited (Meng, You, & Yang, 2018; He, Qiu, Ono, & Qi, 2020; Bhat et al., 2018; Zhao et al., 2016).

Another space-saving highly efficient technology is the high concentrator photovoltaic (HCPV) design. Here, lenses are used to focus sunlight on very small areas of solar cells, which allows the usage of micro high-efficiency cells. HCPV power plants only collect direct normal irradiance (DNI), which makes them less applicable for regions with low DNI. In this study, we investigate the impact of a hybrid HCPV-silicon module developed by Insolight[1] with a silicon flat plate module that collects diffuse horizontal irradiance as well as direct normal irradiance with an angle of incidence (AOI) greater than 60 degrees. Even though HCPV achieves high efficiencies of above 30 %, they are not commercially prevalent yet, because of comparatively high costs (Horowitz, Woodhouse, Lee, & Smestad, 2016; Wiesenfarth, Philipps, Bett, Horowitz, & Kurtz, 2017).

[1] https://insolight.ch/

In addition to the electricity sector, the heat sector plays a major role in the decarbonisation of the energy system. "Heating and cooling in buildings and industry accounts for half of the EU's energy consumption" and fossil fuels dominate heating and cooling applications with 75 %, while only 19 % is generated from renewable energy (European Commission, 2020). According to the European Commission (2020), energy consumption in the heating and cooling sector must be reduced and renewable and environmentally friendly energy sources must be expanded in order to meet the EU's climate and energy targets. One technology that has the potential to further increase grid flexibility, due to coupling the electricity and heating sector, is the heat pump (see a. o. Battaglia, Haberl, Bamberger, & Haller, 2017). The use of a thermal energy storage in combination with a heat pump powered by solar electricity can increase the degree of self-consumption in households (Williams, Binder, & Kelm, 2012; Beck, Kondziella, Huard, & Bruckner, 2017b). According to the report of Nowak, Westring, and European Heat Pump Association (2015), the state-of-art technology of heat pumps used for space heating is air-to-air technology in Spain, while in Germany, there is a trend towards air-to-water technologies.

To analyse the influence of the different PV technologies on urban energy systems, we use the method of energy system analysis with special focus on the potential for net zero energy. Energy system analysis of PV-powered heat pumps is widespread. The modelling of heat pumps with and without thermal energy storage systems is for example performed in the publications Renaldi, Kiprakis, and Friedrich (2017) and Beck et al. (2017b). A detailed study of the parameterisation of a heat pump model for energy system analysis was presented by Ruhnau, Hirth, and Praktiknjo (2019) Lindberg et al. (2016) and Thygesen and Karlsson (2013) further address the modelling of heat pumps in energy systems with a thermal energy storage with focus on the NZE status. D'Agostino, Mele, Minichiello, and Renno (2020) examines the number of PV panels required to achieve a NZEB status for two cities in Italy. In the study, a ground source heat pump is compared with an air source heat pump and a condensing boiler coupled to a chiller. In both cities, the ground source technology is superior to the other two in achieving NZE status.

Concerning concentrating PV, some studies focus on concentrating photovoltaics/thermal (CPV/T) hybrid modules (Hao et al., 2018; Renno, 2014; Renno, D'Agostino, Minichiello, Petito, & Balen, 2019; Ben Youssef, Maatallah, Menezo, & Ben Nasrallah, 2018). Other studies explore concentrator photovoltaics (CPV) in combination with a hydrogen storage (Burhan, Shahzad, & Ng, 2017; Burhan, Chua, & Ng, 2016) or in very specific settings, such as green houses (Sonneveld et al., 2011). Brandoni, Renzi, Caresana, and Polonara (2014) compare the integration of HCPV and polycrystalline silicon (SI) in a hybrid renewable system with combined cooling, heat, and power on three different building typologies (ten-flat apartment building, office, hotel). The systems with SI "provide better results in terms of energy and costs" when the DNI is low and HCPV provides better results "for high DNI values" (Brandoni et al., 2014, p. 675). Renno and Perone (2021, p. 384) analyse the "energy and economic

performances of a point-focus CPV system for a residential user" in three different climatic conditions on typical winter and summer days.

No works on energy system analysis with PSI are known to the authors. However, Yang et al. (2020) compare perovskite-based solar cells with amorphous silicon PV and dye-sensitised solar cells in PV glazing. This work shows that building-integrated PV with perovskite is subject to research, even if not in the context of energy supply.

There are very few studies on the energy supply of NZE buildings with other innovative high-efficient PV technologies. Good, Kristjansdottír, Houlihan Wiberg, Georges, and Hestnes (2016) focus on net zero emission buildings studying silicon and Cadmium Indium Selenide (CIS) modules and dos Santos and Rüther (2012) did a case study with thin-film amorphous silicon and crystalline silicon on detached single-family houses, where all evaluated houses resulted into net energy-positive buildings.

In summary, during the publication of this study, no works on energy system analysis in the sense of analyzing the possibilities of future energy supply and, in particular, the integration of renewable energy with CPV or PSI technology focusing on residential areas in cities, were known to the authors. Neither were a work on the potential of NZE buildings/communities with non-thermal CPV or PSI technologies. Energy system analysis with heat pumps, on the other hand, is widely conducted, but lacks the combined consideration with CPV or PSI.

In this study, we therefore analyse the integration of three innovative technologies into urban energy systems in an energy system analysis with linear optimisation: a hybrid HCPV-silicon module, further called CPV, a fictitious high efficient tandem perovskite silicon module that is based on the 2-terminal tandem perovskite silicon cells from (Chen et al., 2020), further called PSI, and a PV-powered heat pump, further called heat pump (HP). We compare these technologies to state-of-the-art technologies for electricity production: the multi-crystalline silicon PV technology, further called SI, and for heat production, a natural gas fired heating system.

We focus on the local energy system of a fictional residential area (neighbourhood) of 20 buildings under two different climatic conditions in Madrid (Spain) and Berlin (Germany). We analyse the impact of the three technologies (CPV, PSI, and HP) on the local energy system concerning its degree of autonomy, self-consumption, total system costs, and reduction of GHG emissions. Additionally, we explore the potential of these technologies for NZE communities.

Focusing on the electricity sector of the neighbourhood that covers its demand with rooftop PV, and optionally PV on facades, with the option of storing energy in a battery storage, we answer the following questions:

1 a) Under which conditions can the innovative technologies CPV and PSI compete with the state-of-the-art PV technology concerning their costs and lifetime?

1 b) How do these technologies influence the degree of autonomy of the system and how many storeys (households) can be supplied with the respective technologies in an NZE community?

1 c) How do the location of the energy system, and therefore the irradiance, energy price and feed-in tariff affect the results?

In the second thread, we evaluate the sector-coupled energy system in which space heating is supplied by a heat pump that is powered by state-of-the-art SI technology and the grid. Heat can optionally be stored in a thermal storage. The following questions are evaluated:

How does including a heat pump and a heat pump with thermal energy storage into the energy system in case of use for space heating affect

2 a) self-consumption,

2 b) GHG emissions and

2 c) total system costs?

Finally, we compare the sector-coupled systems provided with state-of-the-art PV with sector-coupled systems including the new PV technologies (CPV and PSI) and evaluate the effect of the new PV technologies on the following:

3 a) Does the installation of the new PV technologies add value to the energy supply of the sector-coupled systems with heat pumps? How does the use of the new PV technologies influence the degree of NZE, degree of autonomy, self-consumption, total system costs, and GHG emissions?

3 b) Can the sector-coupled system with a certain amount of storeys be supplied as an NZE community? What impact do the new PV technologies have on the potential for a NZE community?

The study is structured as follows: In section 2, we describe the underlying methods and name data sources used for the energy system analysis. Section 3 depicts the results of the analysis and is structured analogically to the above listed research questions: section 3.1 shows the cost analysis of CPV and PSI and a lifetime analysis for PSI, section 3.2 analyses the potential of the CPV, PSI, and SI technologies for supplying NZE communities, and section 3.3 shows the effect of the location on costs and emissions for all three technologies. To answer research question 2, section 3.4 analyses the sector-coupled energy system with HP and thermal energy storage (TES) supplied with state-of-the-art silicon PV compared to

the reference scenario with gas supply. Finally, the sections 3.5 and 3.6 analyse the sector-coupled system in combination with the innovative PV technologies CPV and PSI and the potential of these technologies for supplying the sector-coupled energy systems as NZE communities in comparison to the SI technology. The conclusion is given in section 4.

2. Methods and Data

We answer our research questions with the method of energy system analysis. The energy system model is shortly described in section 2.1, while the model assumptions are depicted in section 2.2. Section 2.3 describes the scenarios that we have set up for the analysis and section 2.4 defines the key performance indicators used for the evaluation of the results.

2.1. Energy system model

The energy system analysis is carried out with *pvcompare*, a model we have developed for "comparing the benefits of different PV technologies in a specified local energy system in different energy supply scenarios" (Steinbach, Haas, & Gering, 2021). The linear optimisation of the energy system is based on *oemof.solph* (oemof developer group, 2016) of the Open Energy Modelling Framework (oemof) and is applied via the *Multi-Vector Simulator (MVS)*, a tool for assessing and optimizing local energy systems (Hoffmann, Duc, & Haas, 2021). The objective function aims to minimise the system costs while the demand during every time of the year is fully covered. The assumptions concerning the optimisation are described in more detail in the documentation of *MVS* in the section Assumptions. Pre-processing is done in *pvcompare* including the calculation of hourly demand profiles (see section 2.2.2), hourly PV production profiles (see section 2.2.3) and hourly coefficient of performance (COP) profiles of heat pumps (see section 2.2.4). Post-processing is both done in *MVS* and *pvcompare*.

2.1.1. Components

Figure 1 shows the main components of the simulated energy system: electricity and heat demand, PV generation, the national electricity grid, heat pump (HP), battery and thermal energy storage (TES). In addition to these components, we also take a PV inverter and a battery charge controller into consideration. In a reference scenario heat demand is supplied by a gas boiler.

2.1.2. Constraints

All energy system optimisations performed in this study are cost optimisations. In order to portray a reasonable picture of our application of PV systems in net zero energy (NZE) communities, constraints are added that allow to restrict the cost-optimal solution to certain conditions.

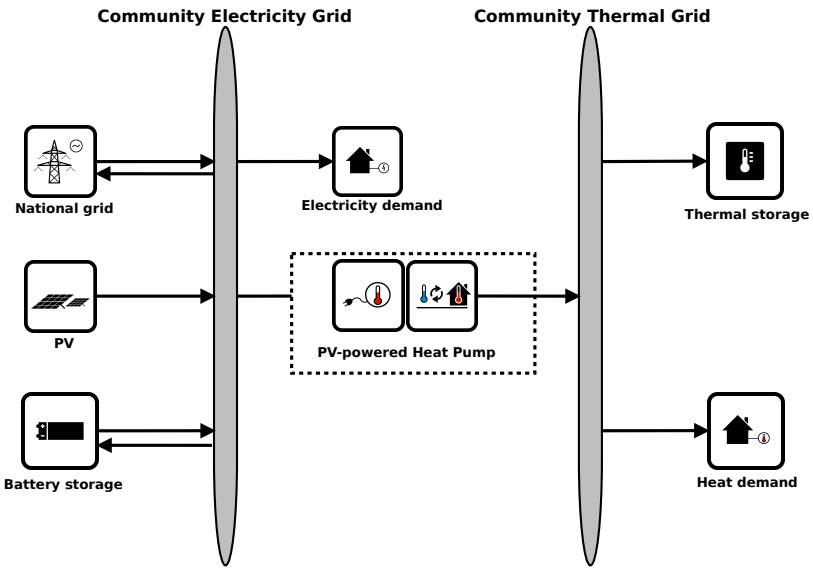

Figure 1: **Simplified diagram of a sector-coupled energy system with demands, PV plant, storages, national grid and heat pump**

The two constraints applied in this study are:

- Maximum capacity constraint
- NZE constraint

The maximum capacity constraint restricts the possible capacity for PV installations to the available rooftop area or facade area, respectively. The maximum capacity is calculated by equation 2 in section 2.2.1.

The NZE constraint requires that grid consumption does not exceed grid feed-in during the period of one year. This results into a degree of NZE ≥ 1 (definition of degree of NZE, see section 2.4.4). The NZE constraint is defined by equation 1:

$$\sum_{i} E_{grid\ feedin}(i) - E_{grid\ consumption}(i) \geq 0 \tag{1}$$

More detailed information on the NZE constaint can be found in the documentation of MVS in section Net zero energy (NZE) constraint.

2.2. Model assumptions

The assumptions of energy system simulations are stated in this section. Section 2.2.1 states the building assumptions, followed by the description of modelling approaches for demand profiles in section 2.2.2, PV in section 2.2.3 and heat components in section 2.2.4. The selection of weather data years for the simulations is depicted in section 2.2.5. Input data that is needed for the modelling approaches are described in the respective section. Remaining input data is referenced in section 2.2.7. Cost estimations for the new PV technologies CPV and PSI are done in section 2.2.6.

2.2.1. Building assumptions

The analysed local energy system is assumed to belong to an urban neighbourhood. The calculation of the demand profiles are based on standard load profiles that are typically generated for 500–1000 households. For more information on the modelling of demand profiles, see section 2.2.2. These load profiles are flattened, compared to profiles of single households. In order to meet the required number of households, we assume a number of 20 buildings for our simulations with a variable number of storeys and a fixed number of eight flats per storey. For five-storey buildings this counts up to 800 households while for three-storey buildings this counts up to 480 households.

The default building parameters are based on the following assumptions that have been adopted from (Hachem, Athienitis, & Fazio, 2014): Each storey with a total area of 1232 m^2 is divided into eight flats of 120 m^2 each. The rest of the storey area is used for hallway and staircases etc. Each of the eight flats is inhabited by four people, meaning in average 30 m^2 per person. Therefore the number of persons per storey is determined to 32. All building parameters can be found in table 1. The number of storeys differs in sensitivity analyses.

Table 1: **Building parameters**

Parameter	Value
Number of storeys	5
Number of houses	20
Population per storey	32
Total storey area	1232 m^2
Length south facade	56 m
Length of east and west facade	22 m
Height of a storey	3 m
Room temperature	20°C
Heating limit temperature	15°C
Include warm water	False

We assume an urban environment that allows high solar exposure without shading from surrounding buildings or trees from the third storey on. Like (Hachem et al., 2014) we assume that PV systems can cover "50 % of the south façade area, starting from the third floor up, and 80 % of the east and west façades". The facades of the first two floors are disregarded for PV installations due to shading. We assume buildings with flat roofs, of which the area available to PV installations is assumed to be 40 % of the total floor area, due to shading between the modules see, Senatsverwaltung für Wirtschaft, Energie und Betriebe and simuPLAN (2011).

With the help of the calculated available area for PV exploitation, the maximum capacity of PV plants is calculated with equation 2. It depends on the module's size and the peak power of the specific PV technology and serves as a constraint for the investment optimisation (see section 2.1.2).

$$\text{maxCap} = (\text{available area}/\text{module size}) \cdot \text{ peak power} \tag{2}$$

2.2.2. Modelling of demand profiles

The load profiles of the electricity and heat demand are generated with *oemof.demandlib* (oemof developer group, 2016), which uses the standard load profiles for households of the German Association of Energy and Water Industries (German: Bundesverband der Energie- und Wasserwirtschaft (BDEW)). Information on these load profiles can be found in the work of Ruhnau et al., 2019.

As there is not much information on other countries' load profiles available, the German standard load profile is used for all locations as an approximation. As in many countries working hours are different, we adapt the demand profiles by shifting working hours, based on (Pezzutto, 2016). For Cyprus, Greece, Portugal, Spain the demand is shifted by +2 hours, for Belgium, Estonia, Ireland, Italy, Latvia, Malta, France, UK by +1 hours and for Bulgaria, Croatia, Czech Republic, Hungary, Lithuania, Poland, Slovakia, Slovenia, Romania by -1 hour.

Electricity demand

To calculate the electricity demand profile, the *H0* BDEW load profile for households is scaled with the annual demand of the population of the neighbourhood. It is assumed that the electricity demand covers not only all electrical demand for lightning and home appliances but also the energy demand for cooling and cooking. For the latter it is assumed that only electrical energy is used for cooking. Therefore, the share of electrical energy consumption for cooking is subtracted from the total electrical energy consumption before adding the

total energy consumption for cooking (see equation 3). We further assume that electricity demand does not cover space heating nor hot water.

The following procedure is taken to calculate the electricity demand profile

1. The total annual residential electricity demand is calculated by equation 3 with the following data for the residential sector taken from Odyssee Project of Enerdata[2]:

    - tec - total electricity consumption of a country (Enerdata, n.d.-d)
    - esh - space heating (Enerdata, n.d.-c)
    - ewh - water heating (Enerdata, n.d.-a)
    - tc - total energy consumption for cooking (Enerdata, n.d.-e)
    - ec - electricity consumption for cooking (Enerdata, n.d.-b)

$$\text{total electricity demand} = \text{tec} - \text{esh} - \text{ewh} + \text{tc} - \text{ec} \tag{3}$$

2. The population of the country is taken from Eurostat, the Statistical Office of the European Union (n.d.-b).

3. To obtain the neighbourhood's total annual demand, the total annual residential electricity demand (step 1) is divided by the country's population (step 2) and multiplied by the neighbourhood's population. The population derives from the number of houses, number of storeys and number of people per storage (for building assumptions see section 2.2.1).

4. The load profile is calculated with *oemof.demandlib* taking holidays into account and then is scaled with the total annual demand of the neighbourhood (step 3).

5. For multiple countries, the load profile is adapted by hour shifting following the approach of HOTMAPS (Pezzutto, 2016).

Heat demand

The heat demand profile is generated by scaling the BDEW standard load profile with the total heat demand of the neighbourhood. We focus on the heat demand for space heating and neglect heat demand for warm water, since the air-to-air HP technology cannot cover it and a comparison with the other two HP technologies would therefore not be possible.

[2] https://odyssee.enerdata.net/database/

Due to the characteristics of the sigmoid function used for the calculation of the heat demand profile in the *oemof.demandlib*, the heat demand never equals zero. Since this does not correspond to the realistic behavior of space heating demand in summer, a heating limit temperature is introduced in our model, above which no heating occurs. The heating limit temperature is set to 15°C by default. If the daily mean temperature exceeds the heating limit temperature the heat demand of that day is removed and distributed equally over the remaining time of the year (see step 5).

To obtain the heat demand profile the following procedure is taken:

1. The residential heat demand (Enerdata, n.d.-f) of a country is taken from the Odyssee Project of Enerdata[3].

2. On the lines of the electricity demand, the population of the country is taken from Eurostat, the Statistical Office of the European Union (n.d.-b).

2. The total residential demand for space heating is divided by the country's population and multiplied by the neighbourhood's population. The population derives from the number of houses, number of storeys and number of people per storage (for building assumptions see section 2.2.1).

3. The heat demand profile is calculated with *oemof.demandlib* for a multi family house and then is scaled with the total annual demand of the neighbourhood (step 3).

4. Heat demand on days with a daily mean temperature above the heating limit temperature of 15°C is removed and distributed evenly over the heat demand profile of the remaining time of the year.

5. For multiple countries, the load profile is adapted by hour shifting following the approach of HOTMAPS (Pezzutto, 2016).

[3] https://odyssee.enerdata.net/database/

2.2.3. Modelling of PV components

The production profiles of the following three PV modules are modelled:

- SI - flat plate PV module with 17 % efficiency
- CPV - hybrid HCPV-silicon module developed by Insolight[4] with 32 % efficiency (Askins, Jost, et al., 2019; Nardin et al., 2020)
- PSI - fictional multi-junction perovskite silicon module (PSI), based on (Chen et al., 2020) with 24.5 % efficiency

Table 2 shows the assumed module size, efficiency and lifetime of the modules. At this stage the lifetime of perovskites is still an important issue of research. The longest reported lifetime of a perovskite cell is only one year (Chang et al., 2018). Nevertheless, we assume that a constant process will be made to achieve lifetimes similar to other PV modules on the market as otherwise they will not be compatible (Sofia et al., 2019). In this study we therefore assume a lifetime of 25 years for PSI. Further, the effects of degradation are neglected for all technologies.

Table 2: **Module size, efficiency and lifetime of the silicon (SI), concentrator photovoltaics (CPV) and perovskite-silicon (PSI) modules used in the simulations**

technology	module size [m^2]	efficiency [%]	lifetime [a]
SI	1.6434	17	25
CPV	0.1	32	25
PSI	1.219	24.5	25

The specific investment costs and operation and maintenance (OM) costs of these three technologies are calculated and defined in section 2.2.6.

In the following, we provide a short description of the modelling approaches for the generation profiles of these three technologies. All detailed assumptions are provided in the documentation of *pvcompare* in section PV Modeling.

SI

The generation profile of silicon PV is calculated with the python-package *pvlib* (Holmgren et al., 2020) for a standard silicon module ("Aleo_Solar_S59y280"). The silicon module parameters are loaded from the cec module database[5]. The generation profile is calculated with the *Modelchain*[6] functionality of *pvlib*.

[4] https://insolight.ch/
[5] https://github.com/NREL/SAM/tree/develop/deploy/libraries
[6] https://pvlib-python.readthedocs.io/en/stable/modelchain.html

CPV

The CPV technology we study in this work is a hybrid micro-concentrator module with integrated planar tracking and diffuse light collection, designed and developed by Insolight. DNI is collected by 1 mm III-V cells, while diffuse horizontal irradiance (DHI) is collected by the back plane SI cell. For an angle of incidence (AOI) not equal to 0°, the biconvex lens maintains focus. "A simple mechanism causes the back plane to follow the focal point" for AOI up to 60° (Askins, Jost, et al., 2019). For AOI > 60° the DNI does not meet the III-V cells anymore and therefore is collected by the back plane SI modules instead. DHI that is not focused onto the III-V cells is collected by the back plane SI cells, as well. The module has a 4-terminal output (Askins, Jost, et al., 2019).

To calculate the CPV generation profile we use the python package *cpvlib*[7]. As this package was under development during the work on our study, we have used a version that was tagged for us[8]. In order to model the dependencies of AOI, temperature and spectrum of the CPV module, the model follows an approach of Gerstmaier, Gómez Padrón, Gombert, Mermoud, and Lejeune (2011). The approach uses the single diode model and adds *utilisation factors* to the output power to account for losses due to spectral and lens temperature variations. The utilisation factors were derived from outdoor measurement data of a three week measurement in Madrid in May 2019. This Data can be found in (Askins, Nardin, Ackermann, Gerlich, & Dominguez, 2019) , whereas the performance testing of the test module is described by Askins, Jost, et al. (2019).

PSI

The generation profile of PSI is calculated with a model that has been developed for this study based on a 2-terminal perovskite-silicon cell studied in Chen et al. (2020). Due to the early stage of development of the technology, no outdoor measurement data was available to draw correlations for temperature or spectral dependencies which are of great impact for multi-junction cells. Therefore, the model is based on cells that have only been tested under laboratory conditions. A schematic picture of the model is shown in figure 2. Input data such as cell parameters, resistance, saturation current, energy band gap and cell size as well as the external quantum efficiency (EQE) curve are adopted from Chen et al. (2020). Further spectral correlations are explicitly calculated by applying Simple Model of the Atmospheric Radiative Transfer of Sunshine (SMARTS)[9] to the given EQE curves of the cell. Temperature dependencies are considered by a temperature coefficient for each sub cell. The dependence of AOI is taken into account by SMARTS. Eventually, losses due to the interconnection of cells to modules are taken into account. This way a module with 24.5 % efficiency and a size of 1.219 m^2 is modelled.

[7] https://github.com/isi-ies-group/cpvlib
[8] https://github.com/isi-ies-group/cpvlib/tree/2020-11
[9] https://www.nrel.gov/grid/solar-resource/smarts.html

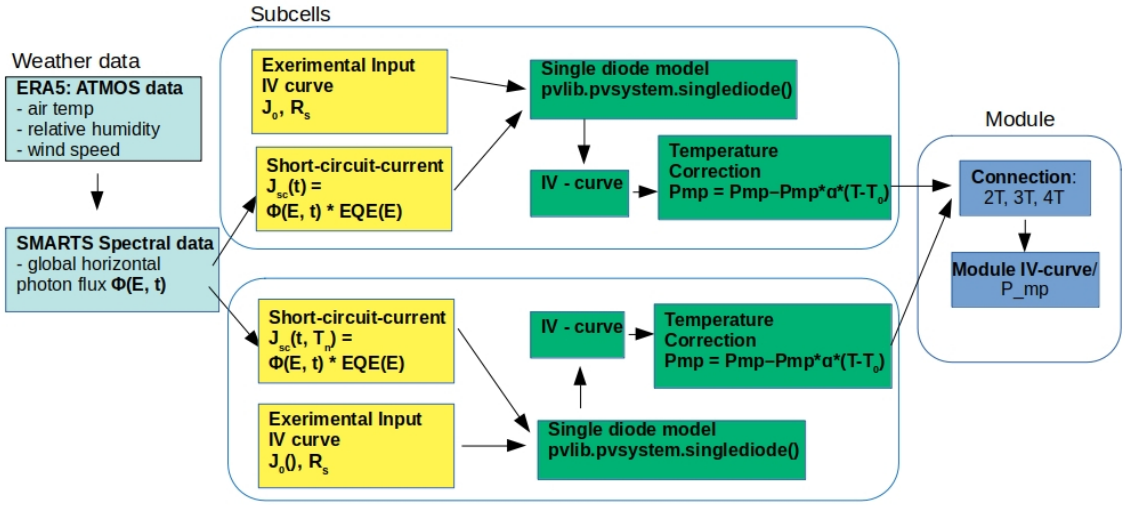

Figure 2: **Modelling scheme of the perovskite-silicon technology**

2.2.4. Modelling of heat components: heat pump, thermal energy storage and gas boiler

The following summarises our assumptions regarding the two heat components, heat pump (HP) and thermal energy storage (TES), and the reference fossil fuel heat component, the gas boiler. The TES can only be combined with the air-to-water HP technology.

The first basic assumption we make is that all heat demand, which is needed for space heating, is covered by the HP. In case of the usage of the air-to-air HP the heat flow is provided by an air stream which flows around the external condenser heat exchanger. We assume an external outlet temperature of the condenser of 28°C and an external inlet temperature of 22°C. In case of the air-to-water technology we model underfloor heating as a method of space heating. We assume a temperature of 40°C as the outlet flow temperature of the air-to-water HP, while a temperature of 34°C is assumed for the inlet flow. In figure 3 the space heating is depicted in case of the use of the air-to-water HP as stand-alone (a) and in case of the air-to-water HP with TES (b).

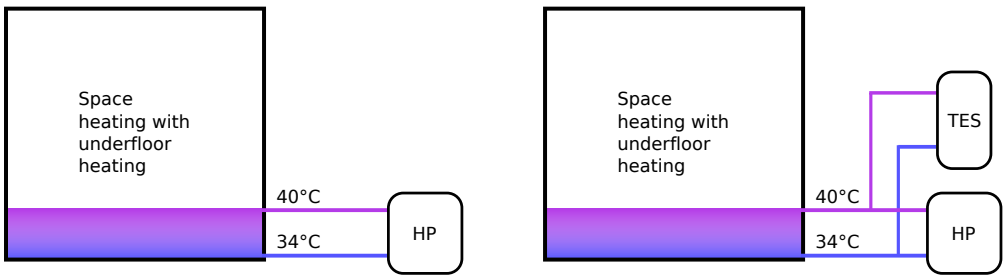

(a) HP as stand-alone (b) HP with TES

Figure 3: **Space heating with heat pump using underfloor heating with inlet and outlet temperatures for the implementation of a HP without TES (a) and with TES (b)**

The temperature difference between internal and external heat exchanger is assumed to be 10 K. The temperatures at the external (left) and internal (right) heat exchangers for the two HP technologies air-to-air (a) and air-to-water (b) are illustrated in Figure 4.

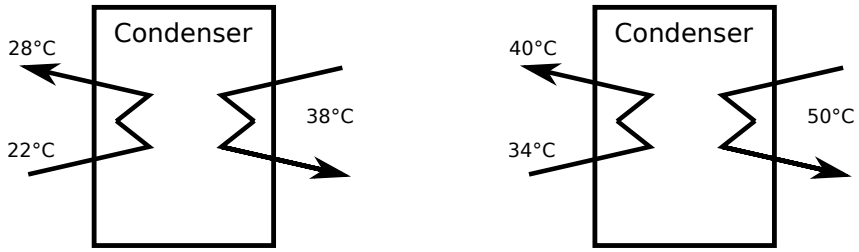

(a) air-to-air HP (b) air-to-water HP

Figure 4: **External (left inlet and outlet) and internal (right inlet and outlet) heat exchanger at the condenser of the HP for air-to-air (a) and air-to-water (b) technologies**

For modelling the HP, its efficiency, the coefficient of performance (COP), is needed to calculate the electric power to be installed from the heat demand. The COP of a dissipative heat engine can be calculated using the Carnot efficiency COP_{carnot} and the quality grade η:

$$COP = \eta \cdot COP_{carnot} \,, \tag{4}$$

where COP_{carnot} corresponds to the ideal efficiency of the heat engine. η is assumed constant for a simple estimation of the COP. COP_{carnot} is defined for the heat pump as follows:

$$COP_{carnot} = \frac{T_1}{(T_1 - T_0)}. \tag{5}$$

T_1 corresponds to the internal outlet temperature of the heat pump condenser. T_0 is the internal inlet temperature of the heat pump evaporator. Substituting 5 into 4 gives:

$$COP = \eta \cdot \frac{T_1}{(T_1 - T_0)}. \tag{6}$$

Furthermore it applies:

$$COP = \frac{\dot{Q}_1}{P_{el}}, \tag{7}$$

with the heating capacity $\dot{Q}_1$ corresponding to the heat flux delivered and the electrical power P_{el} of the heat pump.

Thus, P_{el} can be determined as follows:

$$P_{el} = \frac{\dot{Q}_1}{COP}. \tag{8}$$

In table 3 the assigned parameters of the two technologies of the heat pump are summarised, where T_{amb} is the temperature of the ambience. More information including references on the quality grade η and the external outlet temperature at the condenser T_1 are provided in the documentation of *pvcompare* in section Parameters of pvcompare: Definitions and Default Values.

Table 3: **Overview of the parameters of the two heat pump technologies**

HP-technology	η	T_1	T_0
air-to-air	0.1852	38	T_{amb}
air-to-water	0.403	50	T_{amb}

In our simulations, we use a stratified thermal energy storage with two ideally separated zones. The layout parameters, which are set, are listed in table 4.

Table 4: **Layout parameters of the thermal energy storage (TES)**

	Value	Unit
Diameter	0.79	m
Temperature of warmer stratification (T_H)	40	°C
Temperature of the colder stratification (T_C)	34	°C
Thickness of insulating layer (s_{iso})	100	mm
Thermal conductivity of the insulating layer (λ_{iso})	0.03	W/(m*K)
Heat transfer coefficient of the inner vessel (α_I)	4.3	W/(m²*K)
Heat transfer coefficient of the outer vessel (α_A)	3.17	W/(m²*K)

The height of the storage is optimised together with the storage capacity. For modelling the TES the following three losses are calculated:

- State of charge dependent thermal losses through the lateral surfaces (β),
- Thermal losses through the lateral surfaces in the empty state (γ)
- Constant thermal losses through the lid and bottom (δ)

The efficiency of the TES is determined as follows:

$$\text{Efficiency} = 1 - \beta. \tag{9}$$

The values required for modelling the HPs, the TES and the natural gas boiler with respect to investment are taken from the two catalogues of the Danish Energy Agency (Energinet, 2018, 2016). The parameters are listed in table 5.

Table 5: **Investment-specific parameters of the air-to-air (a/a) HP, the air-to-water (a/w) HP, the stratified TES and the gas boiler (Energinet, 2018, 2016)**

Parameter	Unit	a/a HP	a/w HP	TES	gas boiler
Lifetime	a	12	18	30	20
Specific investment costs	EUR/kW	450	940	410	320
Fix OM costs	EUR/(kW · a)	42.5	29.1	16.67	20.9

2.2.5. Weather data and selection of years

As weather data we use the global reanalysis data set ERA5 which "provides hourly estimates of a large number of atmospheric, land and oceanic climate variables. The data cover the earth on a 30km grid and resolve the atmosphere using 137 levels from the surface up to a height of 80km" (ECMWF, n.d.).

For this study we select three exemplary weather years that show a range of different weather distributions for the locations Berlin and Madrid. In figures 39 and 40 in A.1 the global horizontal irradiance (GHI), direct normal irradiance (DNI) and diffuse horizontal irradiance (DHI) as well as the electricity demand is illustrated for nine years (2010–2018) for Berlin and Madrid. For each year, the annual PV production is calculated and the weather years are sorted based on the energy yield. This way the years 2011 (good), 2013 (bad) and 2016 (medium) are chosen for Berlin and the years 2017 (good), 2013 (bad) and 2015 (medium) are selected for Madrid. Simplistically, we refer to these three years as "good", "medium", and "bad" years. If not stated otherwise, all simulations in this study are performed for these years.

2.2.6. PV cost estimations

In order to include the PV technologies into the energy system optimisation, the specific investment costs and operation and maintenance (OM) costs of the modules have to be defined. Table 6 shows the baseline for the cost estimation for the three technologies SI, CPV and PSI. The total specific investment costs are composed of the module costs and the balance of system (BOS) costs. In the following we give an overview on how the cost estimations are derived.

Table 6: **Cost estimations for specific SI, CPV and PSI rooftop systems in 2019 based on (Fraunhofer ISE, 2015). Cost items with asterisk are scaled (reduced) with the efficiency. The numbers are rounded.**

Parameter / Technology	SI	CPV	PSI
Efficiency [%]	17	32	24.5
Total specific investment costs [EUR/kWp]	934	1019	813
Hardware PV modules	480	750	480
Balance of System costs	454	269	333
Balance of System costs [EUR/kWp]	454	269	333
- Infrastructure*	58	31	40
- Grid connection*	84	44	58
- DC cabeling*	73	39	50
- Installation*	72	38	50
- Mounting*	107	57	74
- Transformer	5	5	5
- Switch gear	20	20	20
- Planning/Documentation	35	35	35
Operation and maintenance costs [EUR/kWp]	20	15	17

Balance of system (BOS) costs

First of all, we derive the BOS costs in more detail and describe how they are estimated for the different technologies.

All BOS cost calculations are done for a commercial rooftop system of about 50 kWp. Fraunhofer ISE (2015) has performed a detailed analysis of the BOS costs for 2015 and future scenarios in 2050 for a 1 MW ground mounted system. Emanating from this study, the costs of all components are extrapolated for the year 2019, following the specific learning curves for each component. In this evaluation a linear regression between 2014 and 2050 and a medium scenario (middle value between worst and best scenario) is considered. As suggested by Vartiainen, Masson, and Breyer (2015), we assume additional 50 % higher BOS costs for commercial rooftop systems (ca. 50 kWp) compared to a 1 MWp ground-mounted system. This way the BOS costs of SI are calculated as given in table 6.

Some of the BOS items depend on the efficiency of the PV module (Fraunhofer ISE, 2015). For simplicity dependencies on DC-voltage and others are neglected. With this information, efficiency dependent BOS item prices for CPV and PSI are scaled according to their efficiencies, see items marked with asterisks in table 6.

Module costs and specific investment costs

Based on the results of Fraunhofer ISE (2015) and Vartiainen et al. (2015) we assume module costs of 480 EUR/kWp for the SI technology. Assuming this price, the total specific investment costs for the SI system sum up to 934 EUR/kWp.

Regarding the module costs of PSI, a few studies have been consulted that investigate the financial perspectives of PSI in the future solar market (Sofia et al., 2019; Li et al., 2018; Lisa Anna, Sebastian, & Jan Christoph, 2020; Chang et al., 2018). While the manufacturing and material costs of perovskites, that are produced using solution-processed thin-film deposition, are very low, the manufacturing and investment costs for wafer-based silicon are quite high. Sofia et al. (2019) and Li et al. (2018) estimate the device manufacturing minimum sustainable price (MSP) for high efficient 4-terminal PSI to be 97 USD/m^2 and 121.18 USD/m^2 (or 82 EUR/m^2 and 103 EUR/m^2 respectively). With a capacity of 245 W/m^2 of the analysed PSI module this results in a MSP of 335 EUR/kWp and 420 EUR/kWp respectively. As a comparison with SI market prices on the one hand and MSP for PSI on the other hand is unrealistic, a market price of 480 EUR/m^2 is assumed, suggesting that the hardware of PSI modules will reach the same price as SI.

Regarding the module costs of CPV, there is diverse information in literature. Kost et al. (2013) reports on total system prices of 1400–2200 EUR/kWp in 2013 for power plants with a capacity of 10 MW. The wide range is caused by a large variety of technological layouts and diverse markets (Wiesenfarth et al., 2017). Further, GTM Research predicts CPV system costs of 1.2 USD/W by 2020 which would result in a price of 1017 EUR/kWp, like evaluated by Kost et al. (2013). Wiesenfarth et al. (2017) report an expected price reduction to 700–1100 EUR/kWp until 2030 if the technologies are being developed further. This would result in a price range of 997–1747 EUR/kWp in 2020, assuming a linear regression. Keeping all of these studies in mind, we assume a module cost of 750 EUR/kWp, resulting in total system costs of 1019 EUR/kWp which fits well with the extrapolations for 2020.

Operation and maintenance (OM) costs

We assume OM costs of 20 EUR/kW/year for a standard commercial rooftop system (see Fraunhofer ISE, 2015). Following Vartiainen et al. (2015), we assume a 50 % dependence on the system area, “ie, the cost decreases with the improvement of module efficiency”. Therefore, we scale 50 % of the OM costs of PSI and CPV systems with their efficiency.

2.2.7. Economic and technological data

Additionally to input data that is referenced in section 2.2, further economic data like operation and maintenance costs of energy system components and further technological data

like efficiencies has been used in this study. References for this data can be found in the documentation of *pvcompare* in section Parameters of pvcompare: Definitions and Default Values. The references are ordered analogous to the input data files of which a collection is provided in the GitHub repository of *pvcompare*.

2.3. Description of scenarios

In order to answer our research questions, several scenarios including sensitivity analysis have been set up for the electricity sector as well as for a sector-coupled system. Table 10 and table 11 in annex A.3, show an overview over the scenarios with their main characteristics and sub scenarios.

2.3.1. Electricity sector scenarios

If not stated otherwise, we use the model assumptions that are described in section 2.2 for all scenarios. With *Scenario A–C* we investigate how different lifetimes of PSI and specific investment costs of PSI and CPV influence the economical competitiveness with the state-of-the-art SI technology, see research question 1a) in section 1. The results of these scenarios are presented and discussed in section 3.1.

Research question 1b) deals with the potential of the respective technologies for supplying the electricity demand of a NZE community. As the available area for PV installations is limited the NZE potential strongly depends on the demand. Therefore, the next scenarios focus on the variation of the number of storeys of the buildings. By varying the number of storeys, the demand changes accordingly, while the available rooftop area stays the same. This way we can analyse how many storeys or households can be supplied by PV energy (*Scenario D*). In order to expand the use case, in a further we take facades into account. As described in section 2.2.1, the facades can only be used for PV installations from the third storey upwards. In *Scenario E* we investigate how the extension to the facades effects the degree of NZE as well as what benefit the facades bring in the cases of the different PV technologies. The simulations results of these scenarios are discussed in section 3.2.1.

For all of the above scenarios the energy system is optimised to the cost-optimal solution. As so far there are no financia incentives for NZE communities, the most economical solution only rarely results in a NZE community. However, a directive of the EU requires all new buildings in the EU to be at least nZEBs since the end of 2020 (Parliament & Council, 2010). In order to investigate the potential for NZE communities in energy systems where NZE is required, we optimise the energy system under a NZE constraint in *Scenario F*. This way the most economical solution that meets the NZE constraint is found. However, in many cases (number of storeys and location of Berlin and Madrid) the constraint cannot be met,

which leads to the optimisation not being solved. To examine by what extend the constraint is missed, we establish *Scenario G*, where we require the maximum available area (rooftop and facades) being used for PV installations. Scenarios *F* and *G* also belong to research question b) and results are displayed and discussed in section 3.2.2.

Finally, to answer research question 1c), we set up twelve sub scenarios (*Scenarios H and K*) for twelve different locations in Europe in order to study the effect of the location on the optimisation results for all three PV technologies. In *Scenario H* we consider the weather data for each location as well as the respective grid parameters. The assumptions and references for the grid parameters for each location can be found in table 9 in annex A.2. To concentrate on the influence of the locations' weather, we set up *Scenario K*, in which the electricity price as well as the feed-in tariff are kept constant for all locations. The results of this evaluation are found in section 3.3.

2.3.2. Sector-coupling scenarios

In the case of sector coupling (see table 11), the electricity sector is coupled with the heat sector by means of the HP. Three sector-coupling scenarios (*A*, *B* and *C*) are compared with uncoupled reference scenarios. In analyses of performances of the electricity sector of the energy system, such as the self-consumption, degree of NZE and degree of autonomy (DA), the scenarios *A*, *B* and *C* are compared with the reference scenario of the electricity sector: *RefE*. When we study costs or GHG emissions, we take as comparison a scenario, in which the space heating is accomplished by means of gas boilers: *RefG*.

In *Scenario A*, the impact of the HP on the self-consumption, the GHG emissions and the total costs of the energy system is investigated. According to Nowak et al. (2015) in Spain, air-to-air HPs are used in most cases for space heating while in Germany there is a trend towards air-to-water HPs. Within *Scenario A* the state-of-art technologies of the HP are simulated at each of the two locations.

In *Scenario B*, we examine the impact of the combination of HP and TES on the same key performance indicators (KPIs) as in *Scenario A*. Since the use of a stratified TES in combination with the air-to-air HP technology is not used due to energetic limitations, the TES in *Scenario B* is only investigated in combination with the air-to-water HP technology for each of the two locations.

In *Scenario C*, we compare the new PV technologies, PSI and CPV, with the standard SI technology. We compare the sector-coupled scenarios with the electricity sector scenarios in terms of the degree of NZE, the degree of autonomy and the self-consumption. Then we turn to a more detailed analysis of the self-consumption, the GHG emissions, and the total system costs with regard to the three PV technologies. Furthermore, in *Scenario C*,

we perform an investigation of the potential of the degree of NZE, the degree of autonomy, and the self-consumption at maximum installed PV capacity and facade installation in a comparison of the three PV technologies.

In section 3.4 we use *A* and *B* scenarios of a sector-coupled system together with the reference scenario of the electricity sector *RefE* and the electricity and heat sector with space heating by means with natural gas *RefG*. In section 3.5 we compare *Scenario D*, which contains the electricity sector only, with *C* and *B* scenarios. Further we compare the new PV technologies in *Scenario C* with the standard technology SI in scenarios *A* and *B*. In section 3.6 we again compare *Scenario C* with the respective heat components and SI in scenarios *A* and *B*.

2.4. Key performance indicators

In order to evaluate the results, we define the following key performance indicators (KPIs), with the help of which the simulation results of the scenarios as well as the sub scenarios are compared.

2.4.1. Levelised costs of electricity

We calculate the levelised costs of electricity (LCOE) of PV with the annuity of the attributed costs, the capital recovery factor (CRF) and the total electricity generation by PV with the following equation:

$$\text{LCOE} = \frac{\text{Attributed costs} \cdot \text{CRF}}{\sum_{t=1}^{8760} E_{generated,PV}} \tag{10}$$

For more information on the CRF, see the documentation of MVS, section Economic Dispatch.

2.4.2. Self-consumption

The self-consumption (SC) is a KPI used to calculate the proportion of locally generated electricity (by PV) that is consumed in the community itself.

$$\text{self-consumption} = \frac{\sum_{t=1}^{8760}(E_{generated,PV} - E_{grid,feed-in} - E_{excess})}{\sum_{t=1}^{8760} E_{generated,PV}} \tag{11}$$

2.4.3. Degree of autonomy

The degree of autonomy (DA) represents the share of the local demand that is covered by locally generated energy (through PV) and therefore is used to evaluate the autonomy of the energy system from the grid. The DA is defined as follows:

$$\text{degree of autonomy} = \frac{\sum_{t=1}^{8760}(E_{generated,PV} - E_{grid,feed-in} - E_{excess})}{\sum_{t=1}^{8760} E_{demand}} \tag{12}$$

In this work, the demand only includes electricity demand. In the case of the sector-coupled system, the heat demand is taken into consideration via the electricity consumption of the HP.

2.4.4. Degree of net zero energy

The degree of NZE is a KPI that can be used to reflect the extent to which the simulated community is composed of net zero energy buildings. A degree of NZE of 1 is achieved when the total annual consumption from and total annual feed-in into the grid is equal. The degree of NZE increases as the grid feed-in increases and the consumption from the grid remains the same or decreases with constant demand of electrical energy.

$$\text{degree of NZE} = 1 + \frac{\sum_{t=1}^{8760}(E_{grid,feed-in} - E_{grid,consumption})}{\sum_{t=1}^{8760} E_{demand}} \tag{13}$$

In this work, the demand only includes electricity demand. In the case of the sector-coupled system, the heat demand is taken into consideration via the electricity consumption of the HP.

More detailed information on the NZE constraint can be found in the documentation of MVS in section Net zero energy (NZE) constraint.

2.4.5. Greenhouse gas emissions

To calculate the total GHG emissions, all aggregated energy flows from generation components, including energy providers, are multiplied by the respective emission factor. Since the consumption of energy converted from PV does not cause GHG emissions, in our case the GHG emissions are calculated from the consumption from the energy providers alone:

$$\text{GHG emissions} = \sum_{t=1}^{8760} \sum_{i} E_{provider,consumption}(i) \cdot f_{Emission}(i) \tag{14}$$

The emission factor $f_{Emission}$ is used to calculate direct emissions from an energy carrier during stationary consumption into CO_2 equivalent emissions. The emission factors used in this work are provided in table 9 in annex A.2

2.4.6. Total costs

The costs of the energy system are evaluated via the total costs of the energy system (total system costs) and the total costs of single components. They are defined as the present value of all costs associated with the whole energy system or the component respectively, e.g. investment costs, operation and maintenance and replacement of components.

More detailed information on the total system and component costs can be found in the documentation of MVS in section Net Present Costs (NPC).

3. Results and Discussion

The goal of this study is to picture the potentials and challenges of the integration of the three innovative PV technologies into energy systems and to evaluate their potential to supply NZE communities. In order to compare CPV and PSI with the SI technology we first take a closer look at the electricity sector only (sections 3.1, 3.2 and 3.3), before analyzing the effects of sector-coupling the energy system with heat pumps and thermal storage (section 3.4). Finally, we depict the influence of CPV and PSI on the sector-coupled energy system (sections 3.5 and 3.6).

3.1. Cost analysis of concentrator and perovskite-silicon and lifetime analysis of perovskite-silicon PV

The three technologies, CPV, PSI and SI, have advantages either in efficiency and therefore saving of space, costs or performance. As PSI is at an early stage of research, its future costs and lifetime are uncertain. Therefore, we investigate how costs and lifetime of PSI effect its competitiveness with the state-of-the-art SI technology considering rooftop applications (section 3.1.2). Further, we explore how a lowering of specific investment costs of CPV effect its profitability compared to SI (section 3.1.3). To evaluate the results it is important to understand the performance of the technologies. Thus, we start with an analysis of their energy yield and LCOE (section 3.1.1).

3.1.1. Energy yield and levelised costs of electricity

In order to get a first understanding of the performance of the photovoltaic (PV) technologies, we analyse their annual production and LCOE. Figure 5 shows the energy yield per kWp (left) and per m^2 (right) for SI, CPV and PSI technologies for Berlin and Madrid in their specific medium year. The years are chosen as medium reference years for the specific location, see section 2.2.5. Of the three technologies, SI has the highest performance ratio (PR) and therefore reaches the highest production per kWp. On the other hand, the production per m^2 is the lowest for SI in both locations due to the larger size of the modules. The high-efficient CPV technology reaches the highest production per m^2 but shows a comparatively low production when looking at the energy yield per kWp due to its low PR. Due to its lower PR, the PSI technology shows a lower production per kWp than SI but reaches higher production per m^2 in Madrid owing to its smaller size. In Berlin the energy yield per m^2 almost equals the one for SI. This shows that the energy yield of PSI depends more strongly on the irradiance than the energy yield of SI. The difference in production per m^2 between CPV and the other technologies is subtle in Berlin and is greater in Madrid.

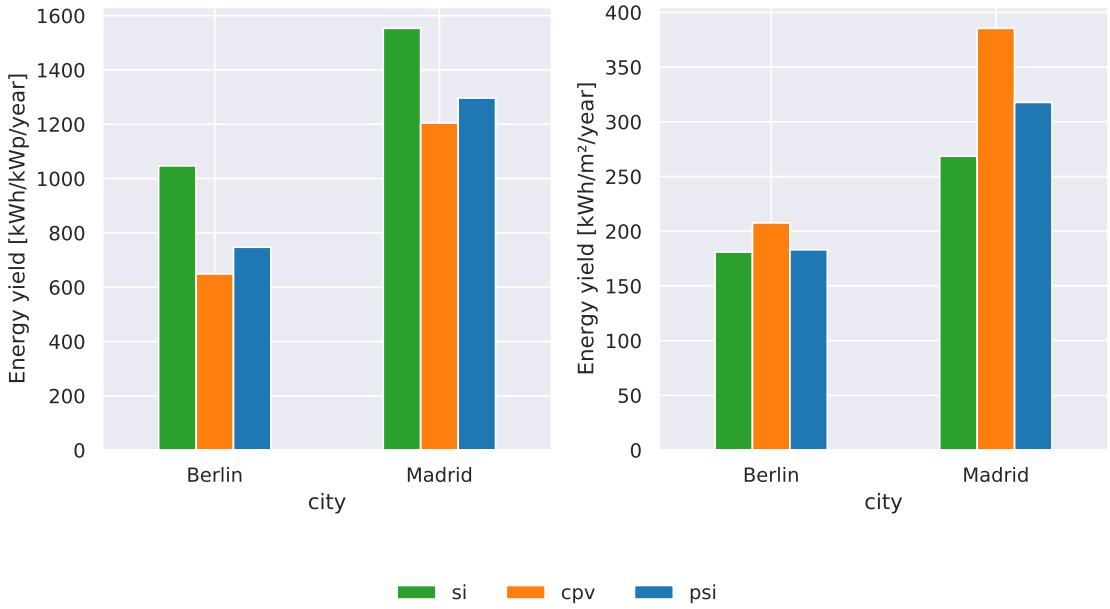

Figure 5: **Energy yield per kWp (left) and per m^2 (right) of SI, CPV and PSI technologies in Berlin and Madrid for the medium weather years, see section 2.2.5 for information on the selected years of weather data**

Additionally to the performance, the costs of the PV technologies play a great role in the energy system optimisation. Figure 6 displays the LCOE of the three PV technologies for three weather years in Berlin and Madrid. The assumptions for the specific investment costs of the PV technologies are displayed in table 7.

Table 7: **Assumed specific investment costs of the three technologies silicon (SI), concentrator photovoltaics (CPV) and perovskite-silicon (PSI), see section 2.2.6 for more information**

Technology	Specific investment costs [EUR/kWp]
SI	934
CPV	1019
PSI	813

In both locations CPV has the highest LCOE due to its high specific investment costs. Even though PSI has lower specific investment as well as operation and maintenance costs than SI, its LCOE is higher. The lower PR of PSI causes that more kWp has to be installed in order to produce the same amount of kWh. It is also interesting to see that the mean LCOE of CPV in Madrid is lower than the the mean LCOE of SI in Berlin. This points out the significance of locations with high irradiance for PV technologies.

Figure 6: **Range of levelised costs of electricity (LCOE) of SI, CPV and PSI in Berlin and Madrid for three weather years**

3.1.2. Sensitivity analysis of costs and lifetime of perovskite-silicon PV

Figure 7 shows the LCOE and the total system costs resulting from the sensitivity analysis with specific investment costs (500–1100 EUR/kWp) and lifetime (5–25 years) of PSI for five-storey buildings. While the LCOE only depends on the energy yield and costs of PSI, the total system costs also depend on the configuration of the optimised energy system. A scenario with the state-of-the-art SI technology is used as a reference, marked with a red dot. Overall, the distribution shows how lower lifetimes and increased specific investment costs lead to higher LCOE and higher total system costs. In case of high costs and low lifetimes (>= 1000 EUR/kWp and <= 5 years in Madrid / >= 800 EUR/kWp and <= 5–8 years in Berlin), it is more profitable to only consume electricity from the grid than to install PSI, so no values for the LCOE are available.

Comparing the LCOEs of each column (all lifetimes at a specific investment cost) with the reference value for SI leads to a reference curve, which is coloured in orange in figure 7. All values above this curve correspond to a lower LCOE, all values below this curve correspond to a higher LCOE compared to SI. For example, for specific investment costs of 600 EUR/kWp, PSI would need to reach a lifetime of at least 17 years in Madrid and of 25 years in Berlin in order to be able to compete with SI. In Madrid this curve has a smaller gradient, allowing for lower lifetimes of down to 12 years with costs of 500 EUR/kWp and reaching 25 years lifetime at higher costs than in Berlin. The margin of costs and lifetime is smaller in Berlin, requiring lifetimes >= 18 years in case of low costs of 500 EUR/kWp and requiring 25 years lifetime at 600 EUR/kWp. This shows that the competitiveness of PSI with SI depends on the irradiance of the location. PSI might still be economically beneficial in locations with high irradiance even in case that only comparably low lifetimes can be achieved if specific investment costs can be reduced.

When looking at the total system costs however, the range of profitable lifetimes reduces to 25 years in Berlin and Madrid at low costs of 500 EUR/kWp. This can be explained by the lower PR of PSI and therefore lower energy yield per kWp, see figure 5. Additionally, in the cost-optimal solution of the energy system in Madrid the installed capacity of PSI is higher than the installed capacity of SI, leading to higher total investment costs.

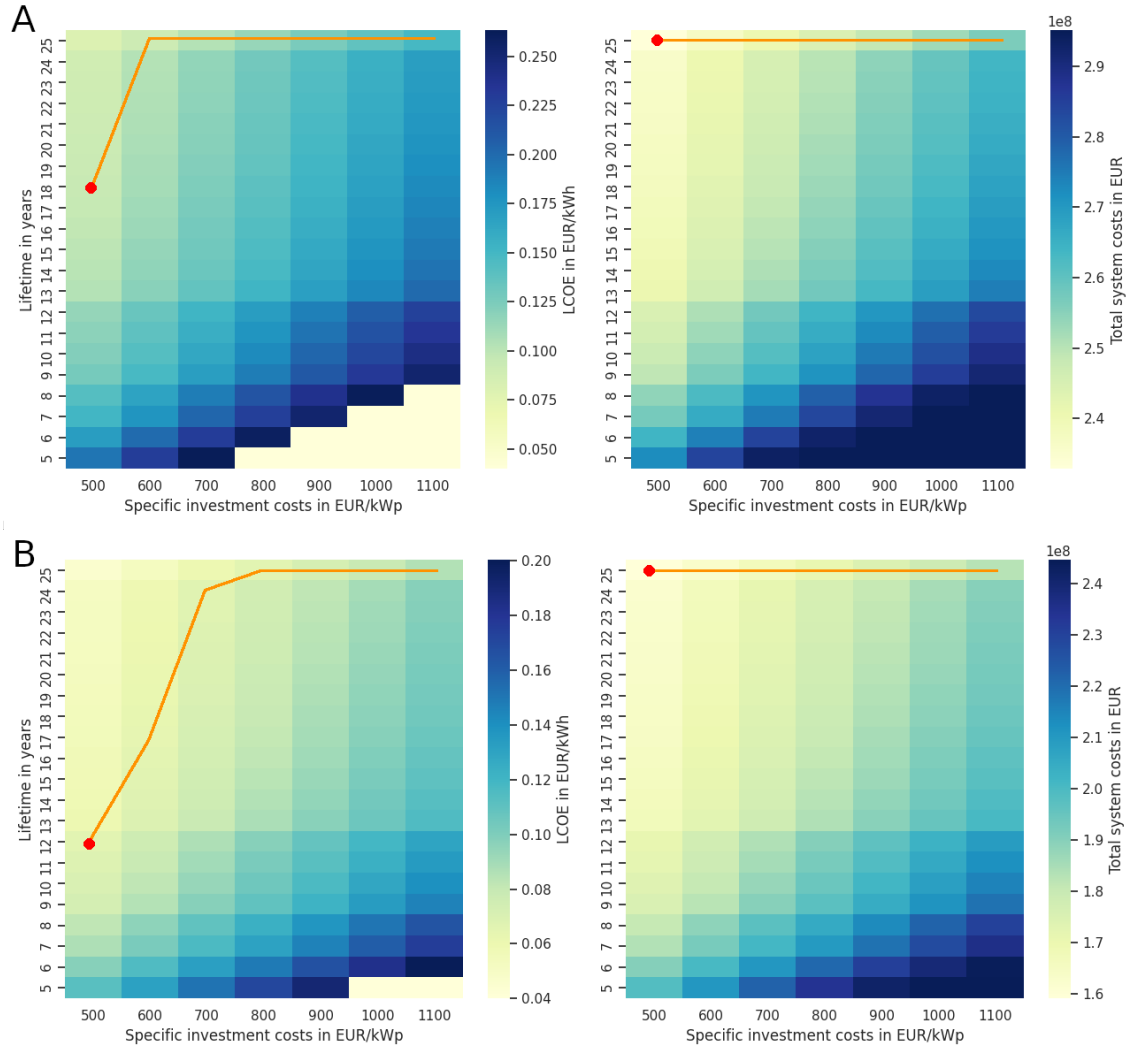

Figure 7: **Sensitivity analysis of specific investment costs and lifetime of PSI for Berlin (A) and Madrid (B) in the specific medium year. The KPIs LCOE (left) and total system costs (right) are evaluated. The reference LCOE (Madrid: 0.0645 EUR/kWh, Berlin: 0.09565 EUR/kWh) and reference total system costs (Madrid: 166669697.75 EUR/kWp, Berlin: 225925957.91 EUR/kWp) of SI are marked with a red dot. The orange line describes the LCOE curve with lifetime values closest to the SI reference value for each specific investment cost.**

3.1.3. Sensitivity analysis of costs of concentrator PV

CPV is a highly efficient but still today very expensive technology (see table 7). With the sensitivity analysis of specific investment costs we display how a variation in costs would effect the competition with state-of-the-art SI. As the lifetime of CPV is not a subject of research and expected to be 25 years like the lifetime of SI, it is not regarded in the sensitivity analysis.

Figure 8 shows the LCOE and total system costs for a range of specific investment costs of CPV between 500–1200 EUR/kWp for Berlin and Madrid. For each location and three weather years the reference value of SI with 934 EUR/kWp specific investment costs is recorded with a dotted line (*Reference - SI*). Overall, the figure shows a constant increase of LCOE and total system costs with rising specific investment costs, as expected. At reference costs of 934 EUR/kWp the LCOE as well as the total system costs of CPV are higher than for SI. The LCOE of SI is met at 550 EUR/kWp in Berlin and 750 EUR/kWp in Madrid. Evaluating the total system costs, CPV requires even lower specific investment costs in order to be competitive with SI: around 500 EUR/kWp in Berlin and around 600 EUR/kWp in Madrid. For both technologies the maximum installable PV capacity is installed. This is almost double the amount of installed capacity (3154 kWp) than for SI (1679 kWp). This leads to much higher investment costs for PV in the case of CPV.

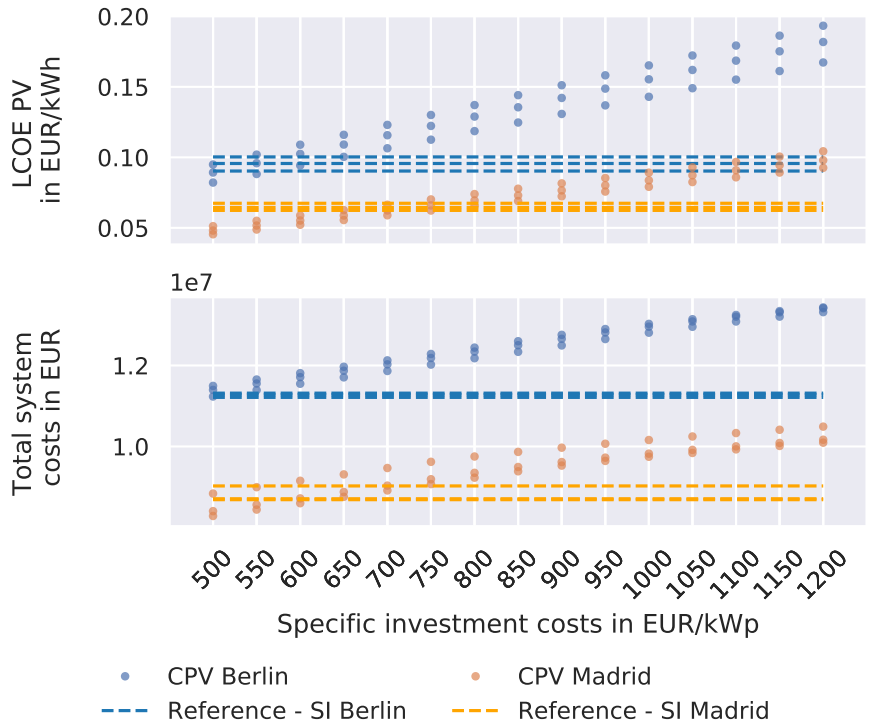

Figure 8: **Sensitivity analysis of specific investment costs for CPV in Berlin and Madrid for three weather years and with reference scenarios for SI**

Eventually, this comparison shows that a usage of CPV is more relevant in locations with high DNI such as Spain, where the total system costs can be reduced by higher energy yields due to increased DNI radiation. However, under current regulations the specific investment costs would have to be reduced in order to compete with the state-of-the-art SI technology. In locations with lower DNI the specific investment costs would need to be reduced drastically in order to be comparable with state-of-the-art SI modules.

3.2. Potential of concentrator, perovskite-silicon and silicon PV for supplying the electricity demand of net zero energy communities

To analyse the potential of CPV and PSI for facilitating a net zero energy (NZE) community in comparison to SI, we investigate how the number of storeys of the buildings with rooftop systems and the additional usage of facades effect the suitability of the three technologies for NZE communities at the locations Berlin and Madrid. In section 3.2.1 we discuss the results from investment optimisations that do not include a constraint, i.e. it is not required to facilitate a NZE community. Then, in section 3.2.2 we examine the results of simulations where the NZE status is required by using a constraint.

3.2.1. Investment optimisation without net zero energy constraint

Figure 9 shows the degree of NZE, the DA and the SC of the cost-optimal solution without requiring a NZE community (no constraint) for a varying number of storeys per building, ranging from 3–8 storeys, for Berlin (a) and Madrid (b). Additional to the flat roof, the south, east and west facades are taken into account for potential PV installations. Each facade is scaled separately within the investment optimisation. In figure 10 the installed capacities of PV and batteries are shown for the same scenario.

The DA is the fraction of the demand that is covered by locally generated energy (autonomy from the grid), while the SC is the fraction of the locally generated energy that is consumed locally. This is the reason why they are influenced in opposite directions with increasing number of storeys when demand and production do not rise with the same proportion (see figure 9). Overall, we can observe a strong correlation between the battery capacity and the DA as higher battery capacities lead to more autonomy from the grid. In Berlin SI shows by far the highest degree of NZE of up to 70 % for three storeys followed by PSI, while CPV only reaches a degree of NZE around 40 % for three to six storeys. In Madrid the degree of NZE is higher for all cases (up to 85 % for SI at three storeys). Here, SI and CPV show similar results of around 50 % for a higher number of storeys while PSI lies a bit below.

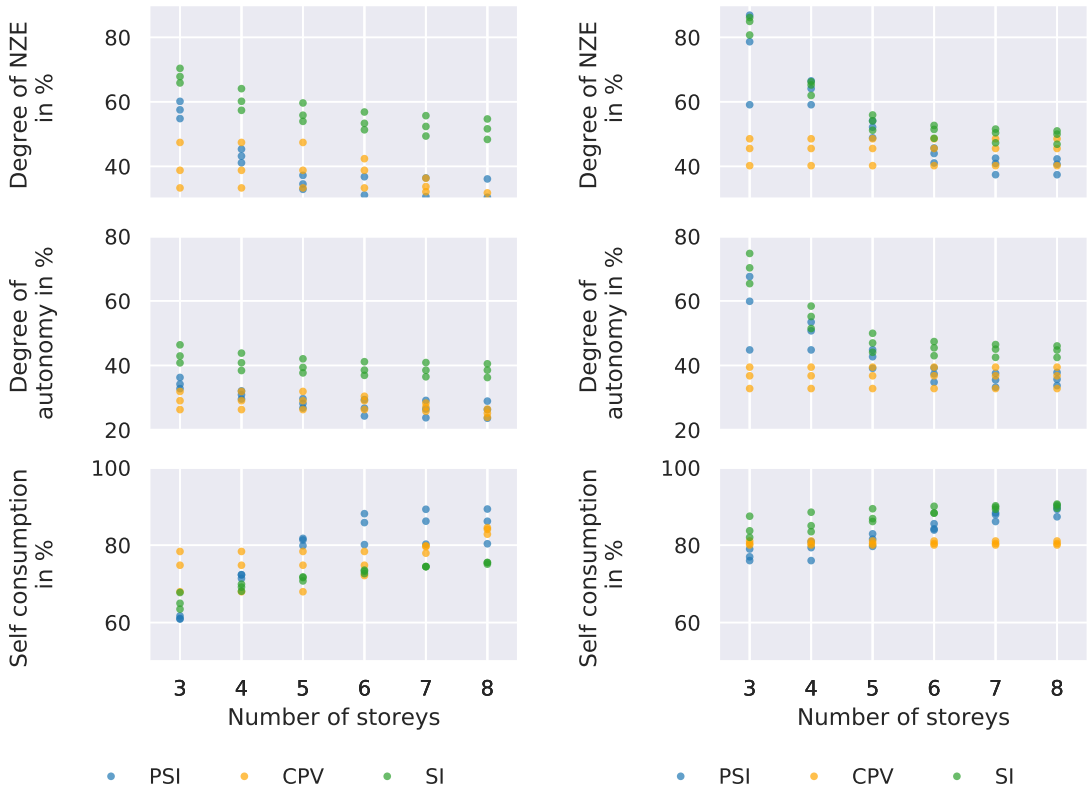

(a) Berlin (b) Madrid

Figure 9: **Degree of net zero energy (NZE), degree of autonomy and self-consumption for the three PV technologies in Berlin (a) and Madrid (b) for varying number of storeys and three years, taking a flat roof and three facades (south, east and west) into account**

For PSI and SI the SC rises with a higher demand in both locations, showing that more of the locally generated energy can be used within the local system. At the same time, the DA is decreasing. This behaviour of SC and DA indicates that the demand increases faster than the generation. For CPV in Madrid the SC as well as the DA and the degree of NZE stay constant for all storey numbers, while the installed capacity rises with the demand. This shows that the local production rises with the same proportion as the demand. The SC of CPV stays with around 80 % lower than the SC for SI and PSI from five storeys on. This indicates that CPV has a higher production of electricity that cannot instantly be used or stored. As a battery is only profitable to a certain limit (see figure 10), extra energy is fed into the grid.

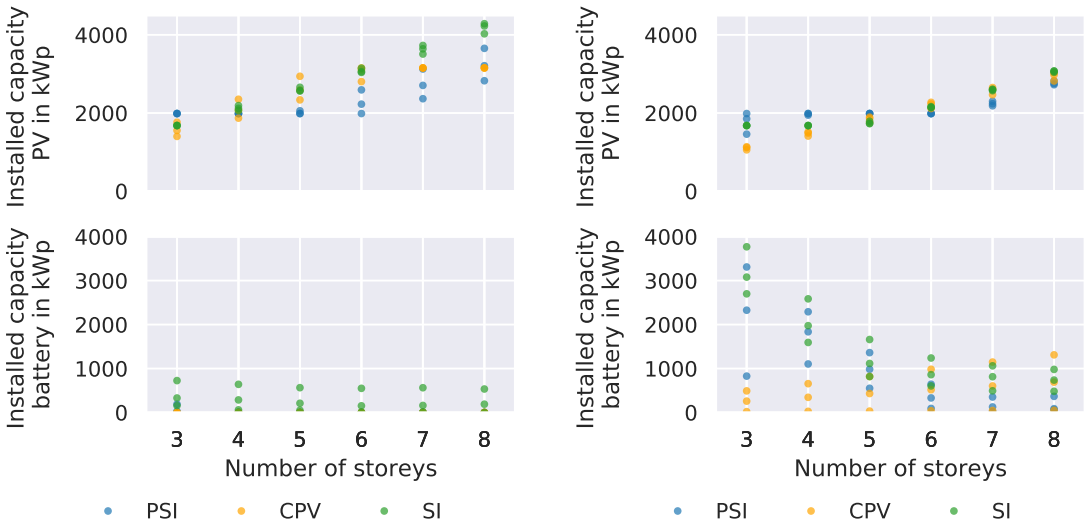

(a) Berlin (b) Madrid

Figure 10: **Installed PV and battery capacity for the three PV technologies in Berlin (a) and Madrid (b) for varying number of storeys and three years, taking a flat roof and three facades (south, east and west) into account**

Interestingly, in Madrid the battery capacity and the degree of NZE for SI and PSI decreases strongly with a rising number of storeys. While at three storeys the degree of NZE is above 80 %, it ranges around 50 % for eight storeys. As most of the locally produced energy can be consumed directly (see increase in SC), battery capacity becomes redundant. The DA of CPV at seven and eight storeys is lower than of SI, while the degree of NZE is similar, reinforcing the observation that there is more grid feed-in for CPV.

In figure 11 the installed capacity, the total annual production and the LCOE of the three PV technologies of a eight-storey building are shown for each facade and the rooftop for three weather years in Berlin (a) and Madrid (b). The crosses illustrate the maximum capacity of the surfaces for each technology. As expected, the installation on rooftops is still the most profitable concerning LCOEs for all three PV technologies in both locations. Overall all facade installations have a higher LCOE than the rooftop installations because of a lower

incoming irradiance and performance. Installations become unprofitable when the LCOE of PV together with the LCOE of the solar inverter are lower than the electricity price.

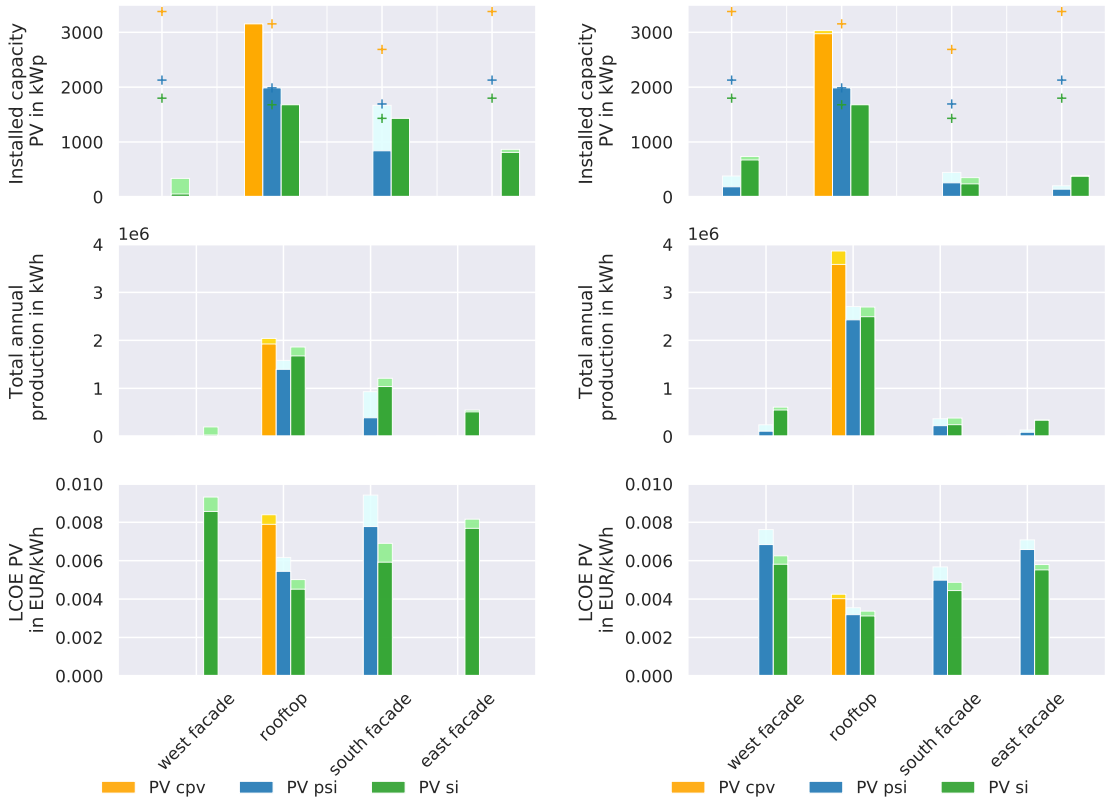

(a) Berlin (b) Madrid

Figure 11: **Installed capacity, total annual production and LCOE of the three PV technologies on different facades and the flat roof in Berlin (a) and Madrid (b) for three years. The light colour indicates the maximum value, the dark colour the minimum value for each KPI. The maximum surface/facade capacity of each PV technology is marked with a cross.**

In Berlin the west facade is used the least, while the south facade is used the most for SI and PSI. In Madrid the west facade is used the most for SI. This is interesting, because it shows the highest LCOE compared to the other facades. This might be due to the fact that the west facade production fits the demand in the evening well, so that the self generated energy can be consumed directly. For PSI the south facade shows a slight advantage compared to the west and east facade (Madrid).

3.2.2. Investment optimisation with net zero constraint / maximum PV capacity installed

The previous results show that none of the three PV technologies reach a NZE community when it is not required in the optimisation. To evaluate the potential for NZE in case of regulations that do require NZE, we analyse the same scenarios with NZE constraint in this sec-

tion (e.g. see EU directive on nearly zero energy building mentioned in section 1). Figure 12 shows the optimised installed PV capacity for a varying number of storeys for Berlin and Madrid for simulations with NZE constraint. It can be seen that in Berlin a NZE community can only be realised when reducing the number of storeys to two, while in Madrid CPV is the only technology that can supply the demand of eight-storey buildings as NZE community. In all other cases the locally produced electricity cannot level the demand over the period of one year. Thus, in these cases the optimisation stops without result (no PV capacity shown in figure 12).

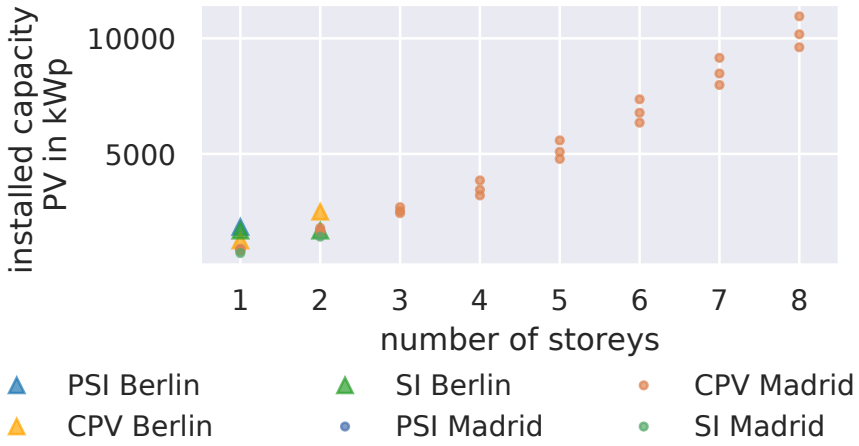

Figure 12: **Installed PV capacity over a varying number of storeys for three PV technologies and three years in Berlin and Madrid with allowed usage of the south, east and west facades and under NZE constraint. For scenarios that miss the NZE constraint no installed capacity is displayed.**

To display to which extend the NZE status is missed for these cases, we evaluate the degree of NZE of energy systems with the maximum PV capacity installed that is available on rooftops and facades (south, east and west facade). Further, we call this scenario the maxCap scenario, in order to distinguish it from the NZE constraint scenario (figure 12) and the investment optimised scenario without NZE constraint (section 3.2.1). Figure 13 shows the results of the maxCap scenario for different KPIs in Berlin and Madrid.

Interestingly, in the maxCap scenarios, the NZE constraint is excelled by far for the first storey in Berlin and Madrid, reaching a degree of NZE of around 200 % for the three PV technologies in Berlin and up to 400 % for CPV in Madrid. For more than two storeys, the degree of NZE of SI and PSI as well as of CPV in Berlin levels off slightly under 100 % and keeps constant for all storeys. So, even though a NZE community is not achieved for buildings with three and more storeys (except for CPV in Madrid), degrees of NZE of 57–78 % in Berlin and 82–112 % in Madrid can be reached for a number of eight storeys and the medium year (see table 8).

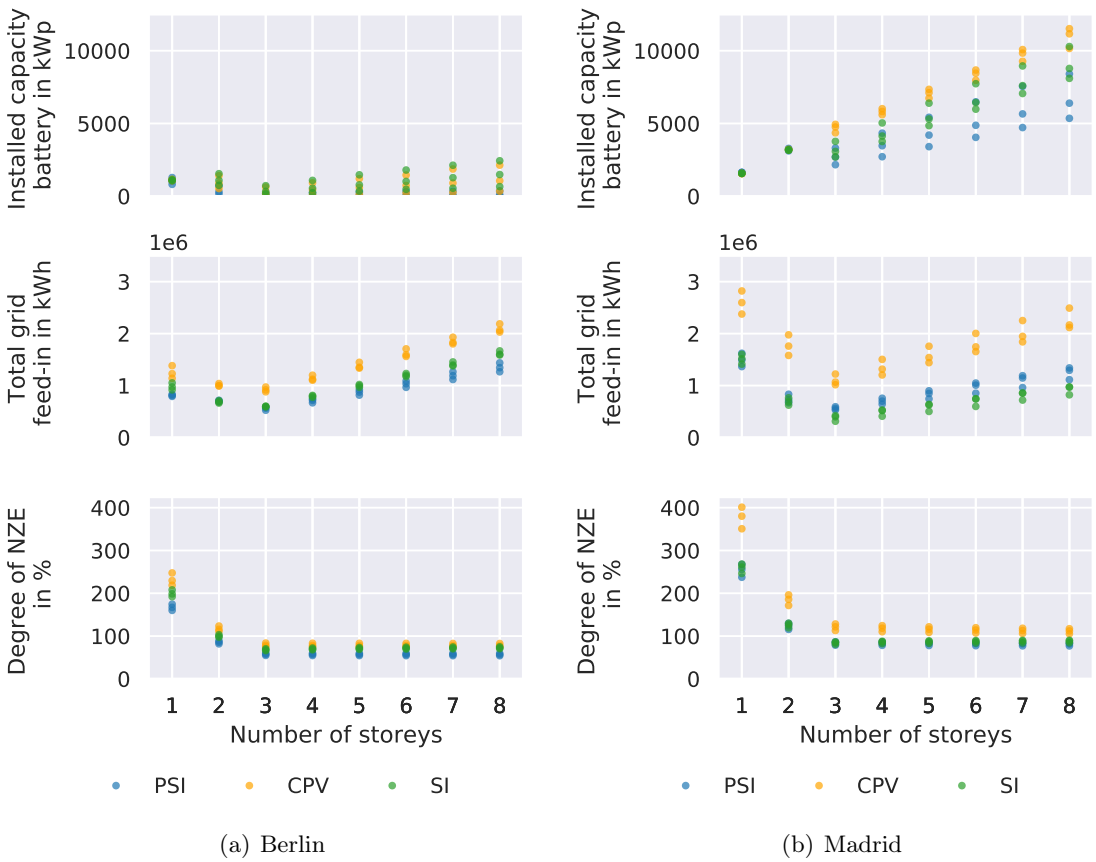

(a) Berlin (b) Madrid

Figure 13: **Installed battery capacity, total grid feed-in and degree of NZE over a varying number of storeys for three PV technologies and three years in Berlin (a) and Madrid (b) of scenarios having the maximum PV capacity installed on rooftops and facades (maxCap scenario)**

Table 8: **Degree of NZE for scenarios with the maximum PV capacity installed on rooftops and facades (maxCap scenarios). The values correspond to eight-storey buildings and the medium weather year of the location.**

Technology	Degree of NZE in Berlin in %	Degree of NZE in Madrid in %
SI	72	89
PSI	57	82
CPV	78	112

In both locations the battery capacity as well as the grid feed-in increases with the number of storeys (from three storeys on). With a rising installed PV capacity (on facades) both, the locally consumed energy as well as the electricity that can be fed into the grid increases. The installed battery capacity in Madrid is five times higher than in Berlin, reaching over 10000 kWp for CPV.

Figure 14 compares the total system costs of the investment optimised scenarios (a1 and b1, see section 3.2.1) and the maxCap scenarios (a2 and b2) for Berlin (a) and Madrid (b). The total system costs of all scenarios increase with the number of storeys, as expected, while CPV induces the highest system costs, followed by PSI and SI. A lowering of specific investment costs of PSI and CPV as discussed in chapter 3.1 would increase the significance of these technologies in terms of costs, which has a great impact on the competitiveness.

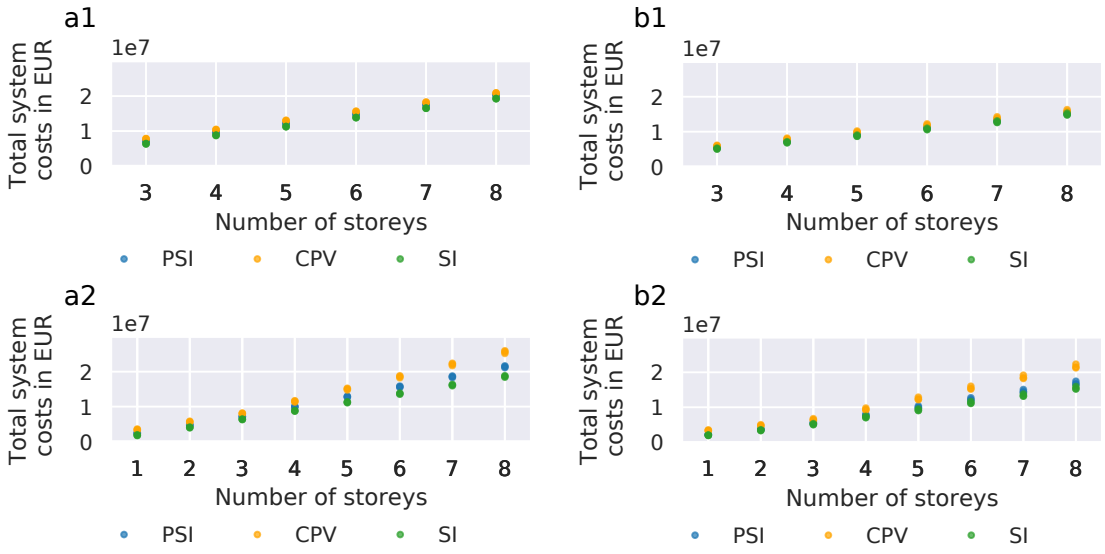

(a) Berlin (b) Madrid

Figure 14: **Total system costs of the investment optimised scenarios (a1 and b1, see section 3.2.1) and the maxCap scenarios (a2 and b2), where all available rooftop and facade area is used for PV installations, for Berlin (a) and Madrid (b). All simulations are performed for a varying number of storeys and three weather years, while all facades are considered.**

Comparing the total system costs of the maxCap scenarios (a2, b2) with the investment optimisation scenarios (a1, b1) it becomes clear that the systems reaching or coming close to NZE are only slightly more expensive. In Berlin the investment optimised scenario of SI has only 1.6 % less mean total system costs, while CPV has 18.6 % less mean total system costs for a number of eight storeys. In Madrid the investment optimisation scenarios result into 26.7 % less mean total system costs for CPV and 6.2 % less mean total system costs for SI. For CPV this number accounts for a degree of NZE of 112 % though. Compared to the NZE constraint scenario in Madrid, where a degree of NZE of 100 % is reached (see figure 12), the investment optimised scenario has only 21 % lower mean total system costs. For PSI

the total system costs lie between the ones of SI and CPV, while in Madrid they are close to the results of SI.

Figure 14 shows that in the case of SI in Berlin and Madrid as well as in the case of PSI in Madrid, a comparatively small increase of the costs of less than 10 % would have a great effect of the facilitation of nZEB communities, almost reaching NZE. SI reaches a higher degree of NZE than PSI at lower costs. However, due to the low technological readiness level (TRL) of PSI the assumptions for its module costs are still quite uncertain (also see section 2.2.6). If costs of PSI can be reduced they might be a good alternative for SI. CPV remains the only technology that enables a complete NZE community. In areas where space is an issue and where possibly facades might not be available for PV installations, e.g. due to shading, CPV allows for the maximum yield of production.

3.3. Influence of the location on costs and emissions of an energy system supplied with electricity from concentrator, perovskite-silicon and silicon

In this section we show how different European locations and their weather conditions effect the energy system optimisation results for the three technologies CPV, PSI and SI. In a first analysis the weather conditions and GHG emissions per kWh of the grid electricity are adapted whereas values for electricity price (0.2 EUR/kWh) and feed-in tariff (0.1 EUR/kWh) are kept constant (see figure 15). This way we study the influence of the weather conditions neglecting the different regulations of the locations. In another analysis each country's local grid parameters are added to the simulations, displaying a more realistic picture of the status quo (see figure 16). The country specific values for the political conditions / grid parameters can be found in table 9 in section A.2. For countries that do not have a feed-in tariff, the default value of 0.05 EUR/kWh is used (see table 9). The comparison of both scenarios allows for a wider picture of potential usage of the PV technologies in different regions and their actual profitability under today's conditions. We consider only the electricity sector in these examinations.

In figure 15 the total annual production of the PV plants, the installed capacity, the total system costs and the total GHG emissions of the energy system are displayed for 12 European locations and three different PV technologies with constant grid parameters. It is remarkable that for all countries and weather conditions all PV technologies are profitable with the given grid parameters. In all locations except of Warsaw, Poland, Manchester, UK and Riga, Latvia the maximum capacity of PSI plants is installed and in all locations the maximum capacity of SI is installed. Because of the consistent installed capacity, the total annual production displays the dependency of weather conditions for these two technologies very well. While northern locations (Helsinki, Manchester, Berlin, Riga) show a comparably low annual production around of 1.7 GWh, more southern locations like Athens, Rome, Sevilla or Madrid show a higher production of around 2.5 GWh.

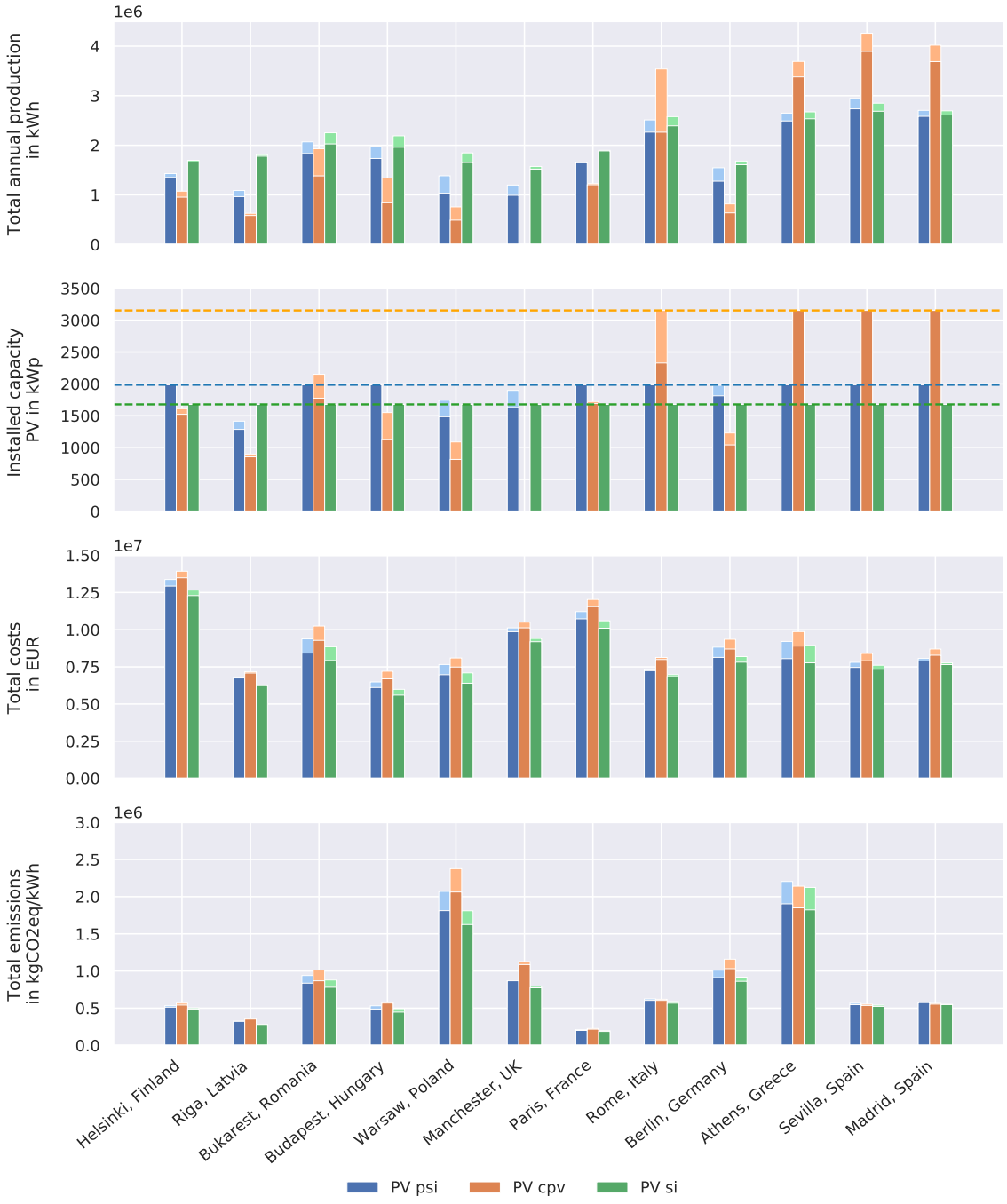

Figure 15: **Total annual PV production, installed PV capacity, total system costs and total GHG emissions for 12 locations in Europe for two exemplary years (2014 and 2017). While the weather data as well as the GHG emissions of the grid electricity are adapted for each location, the electricity price (0.2 EUR/kWp) and the feed-in tariff (0.1 EUR/kWh) are set constant for all locations. The lowest values are coloured in dark while the highest values are shown in light colours.**

For CPV the maximum capacity is a lot higher than for SI and PSI owing to its space-saving and high efficient characteristic. It can be seen that only in locations with high DNI like Rome, Athens, Sevilla and Madrid it is profitable that the whole available area with over 3000 kWp is used for CPV. In more northern countries (all except of Rome, Athens, Sevilla and Madrid) CPV is less profitable than SI and PSI, while in Manchester it is not installed at all. When comparing the total system costs of the PV technologies for each location it becomes clear that implementing CPV results in the most expensive energy systems, followed by PSI and SI. In figure 16 all local grid parameters such as feed-in tariff, electricity price, emissions of the specific countries are taken into account. A low local electricity price and/or a low feed-in tariff makes the usage of PV unprofitable in many countries.

Comparing the GHG emissions of both scenarios, it becomes clear that they depend on the local grid parameters, but not strongly. In some locations like Riga, Paris, Manchester and Athens they only differ slightly or not at all. In other locations like Warsaw and Bukarest the GHG emissions are higher in simulations with local grid parameters as less PV capacity is installed, e.g. due to the low feed-in tariff. In Berlin more CPV capacity is installed when assuming local grid parameters due to the higher electricity price which leads to a lowering of GHG emissions. The total costs differ between the two scenarios depending on the local grid parameters, e.g. in Berlin the total costs are higher as the local electricity price is higher than 0.2 EUR/kWh.

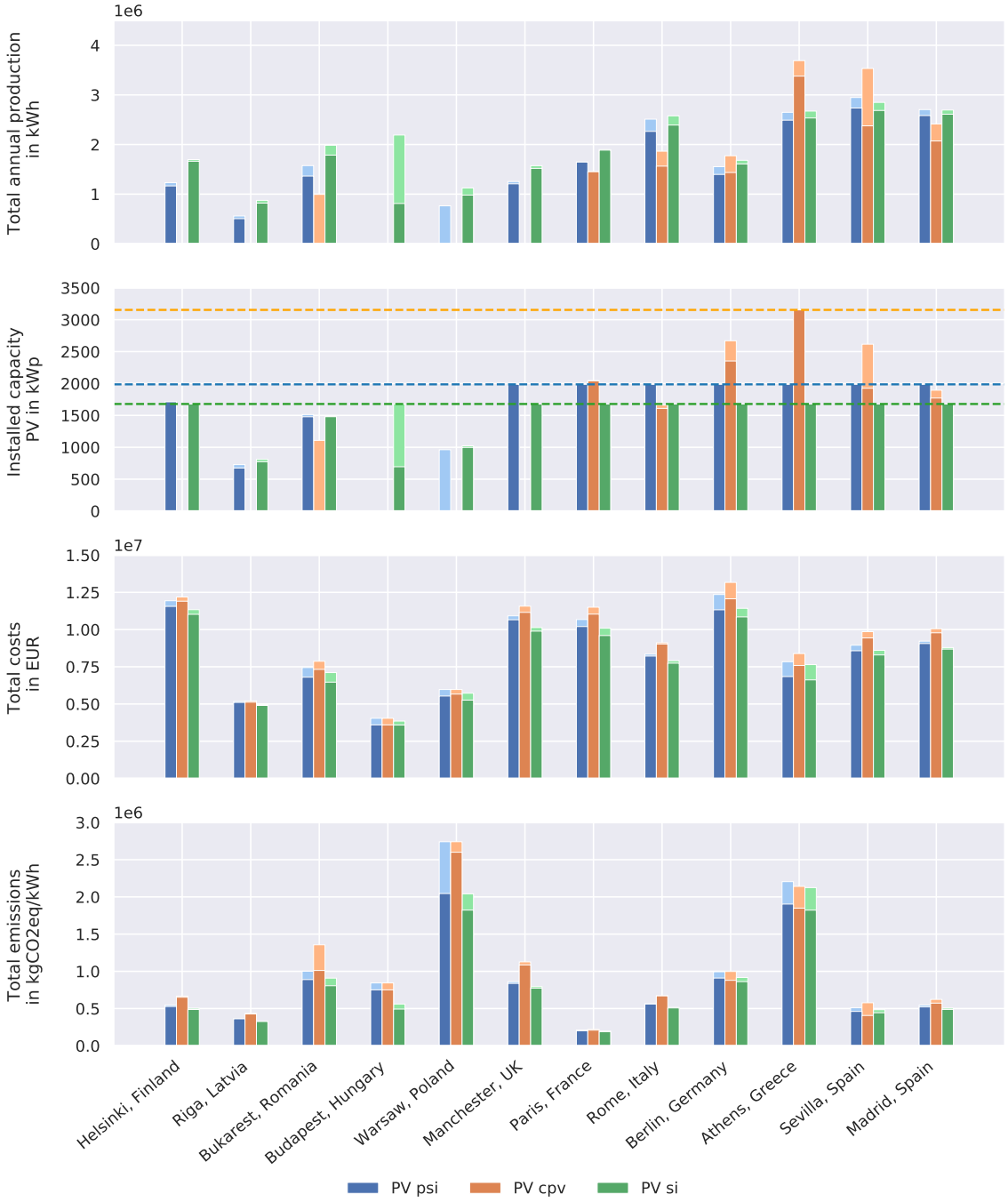

Figure 16: **Total annual PV production, installed PV capacity, total system costs and total GHG emissions for 12 locations in Europe for two exemplary years (2014 and 2017) with local grid parameters. The lowest values are coloured in dark while the highest values are shown in light colours.**

3.4. Analysis of the sector-coupled energy system with heat pump and thermal energy storage supplied with state-of-the-art silicon PV in comparison to the reference scenario with gas supply

Supplying the heat demand of an energy system with a heat pump (HP) may increase the self-consumption (SC) of the system, which may lead to financial benefits depending on the regulations. Thus, we analyse how the integration of a HP, as well as the integration of additionally a thermal energy storage (TES), influence the SC compared to the electricity only system. We further evaluate whether the sector-coupling can lower the greenhouse gas (GHG) emissions compared to an uncoupled system with space heating through gas and additionally compare the total costs of the energy systems. We consider three configurations of the sector-coupled system: air-to-air HP as common technology in Spain, air-to-water HP as common technology in Germany and a system with air-to-water HP including a TES. All three configurations are examined for both locations to be able to compare the results between the locations.

3.4.1. Self-consumption of the energy system

Figure 17 shows the self-consumption (SC) of the scenarios of Berlin (a) and Madrid (b) with air-to-air HP (A1/A2), air-to-water HP (A3/A4) and air-to-water HP with TES (B1/B2) for the minimum and maximum results of the analysed weather years. In comparison the electricity only systems (RefE1/RefE2) are depicted. Analyzing the SC over the scenarios of Berlin (see figure 17a), we find that the SC is higher in the case of the sector-coupled systems (A1, A3 and B1) by 10.8 % on average (over the three simulated years and scenarios A1, A3 and B1) in comparison to the reference scenario (RefE1). The standard deviation of the SC within the scenarios of the sector-coupled system is with 0.4 % comparatively low. In the case of Madrid (see figure 17b) we find a slightly lower SC in the case of the sector-coupled systems (A2, A4 and B2) in comparison to the reference scenario (RefE2) (percentage deviation on average 2.9 %). Also here the standard deviation between the scenarios of a sector-coupling system is relatively low with 0.3 %.

In the invest optimisation an electricity excess is modelled. This is because the capacity of the solar inverter is optimised as well. In case the inverter's capacity is lower than the power generated by the PV modules, the electricity exceeding this capacity is assigned to the excess. The lower the grid feed-in and the electricity excess, the higher the SC (see section 2.4.2). In figure 18 we therefore examine these two KPIs, the total excess electricity and the total grid feed-in, in the scenarios of Berlin (a) and Madrid (b).

(a) Berlin (b) Madrid

Figure 17: **Self-consumption in the scenarios of Berlin (a) and Madrid (b) with A1/A2: air-to-air HP, A3/A4: air-to-water HP, B1/B2: air-to-water HP with TES and RefE1/RefE2: reference scenario of electricity sector**

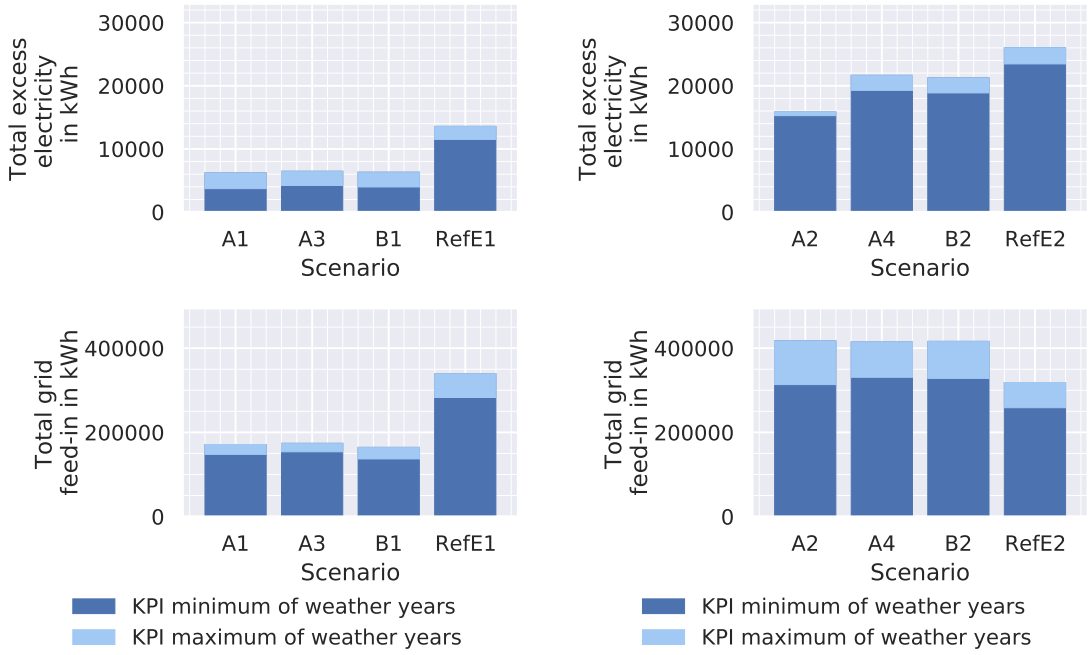

(a) Berlin (b) Madrid

Figure 18: **Total excess electricity and total grid feed-in in the scenarios of Berlin (a) and Madrid (b) with A1/A2: air-to-air HP, A3/A4: air-to-water HP, B1/B2: air-to-water HP with TES and RefE1/RefE2: feference scenario of electricity sector**

For Berlin (see figure 18a) the electricity excess and the grid feed-in are reduced in each scenario of the sector-coupled system (A1, A3 and B1). The electricity excess is lower by 56.1 % on average compared to the reference scenario (RefE1). It is further lowest with the air-to-air technology (A1) followed by the combination of the air-to-water HP and TES (B1) and the air-to-water HP (A3). The deviation within all sector-coupled systems is moderate with a standard deviation of 228 kWh. The total grid feed-in can be lowered by 49.2 % on average in respect to the reference scenario. In the case of Berlin the total grid feed-in is lowest for the combination of a air-to-water HP and TES (B1), followed by the air-to-air HP (A1) and the air-to-water HP (A3). The standard deviation of the sector-coupled systems amounts to 6209 kWh.

Madrid has a higher total excess electricity and grid feed-in than Berlin in almost all scenarios (see figure 18b), primarily due to the amount of energy generated by PV through higher irradiation. The installed capacity is the same with the maximum capacity in both cases, Berlin and Madrid. As for the electricity excess, there is a greater deviation between the air-to-air (A2) and the air-to-water (A4 and B2) technologies compared to Berlin. On average, the excess of electric energy is lower by 24.4 % in the scenarios of the sector-coupled system (A2, A4 and B2) compared to the reference scenario (RefE2). In the case of the air-to-air HP (A2) it is lowest with an average of 37.8 % in comparison to RefE2. The standard deviation of the total excess electricity in the sector-coupled scenarios of Madrid is on average 2916 kWh, which is higher than the one calculated in the Berlin scenarios. The standard deviation of the total grid-feedin amounts to 4333 kWh and thus the deviations within the sector-coupled scenarios are lower than in the case of Berlin.

The total grid feed-in in the sector-coupled scenarios in the case of Madrid is higher compared to the reference scenario, unlike in Berlin. Therefore the SC decreases slightly in comparison to RefE2 (see figure 17). The grid feed-in increases not only because of higher irradiation in Madrid, but also because in the case of sector-coupling the installation of an electric battery is not profitable, optimizing the costs of the energy system. In times when the ambient temperature is below the heating limit temperature, the demand for electric energy of the HP in the sector-coupling scenarios is high, so neglectable or no feed-in occurs. In the period when there is no heating, there is no consumption by the HP and the additional electrical energy is fed into the grid. Over the year, the grid feed-in is larger in the case of sector coupling with HP due to the high density of feed-in in the summer months in comparison to the reference scenario with battery.

These correlations can be observed comparing charging and discharging of the battery with electric energy as well as the grid feed-in and the electricity demand of the HP exemplary for the year 2013 for the scenario RefE2 (figure 19) and scenario A2 (figure 20). In scenario RefE2 in figure 19, there is no electricity demand of the HP but feed-in into the grid all year round. In scenario A2, in figure 20, which was chosen for the comparison, there is no charge and discharge of a battery, but there is a demand of HP for electrical energy. The grid feed-in

occurs approximately exclusively in summer months. Furthermore, it can be seen that the density of the energy fed into the grid is higher in the case of A2 compared to RefE2.

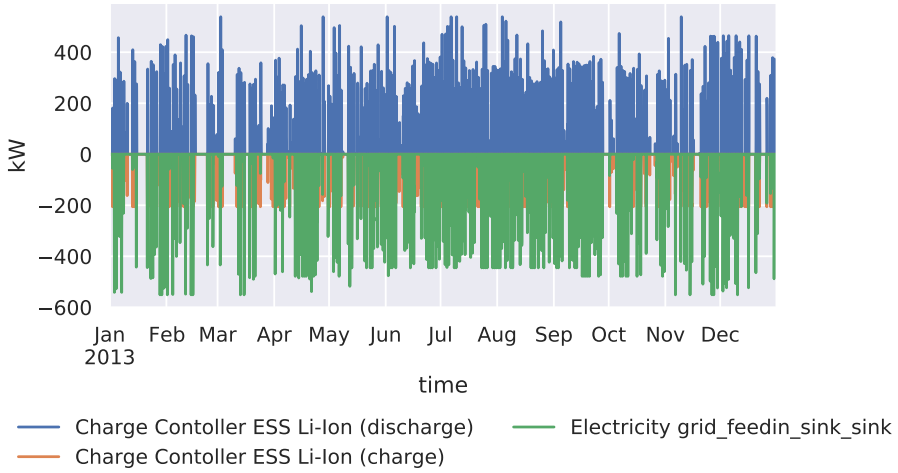

Figure 19: **Charge and discharge flows of ESS Li-ion battery and grid feed-in of electricity of scenario RefE2 (in bad weather year in Madrid)**

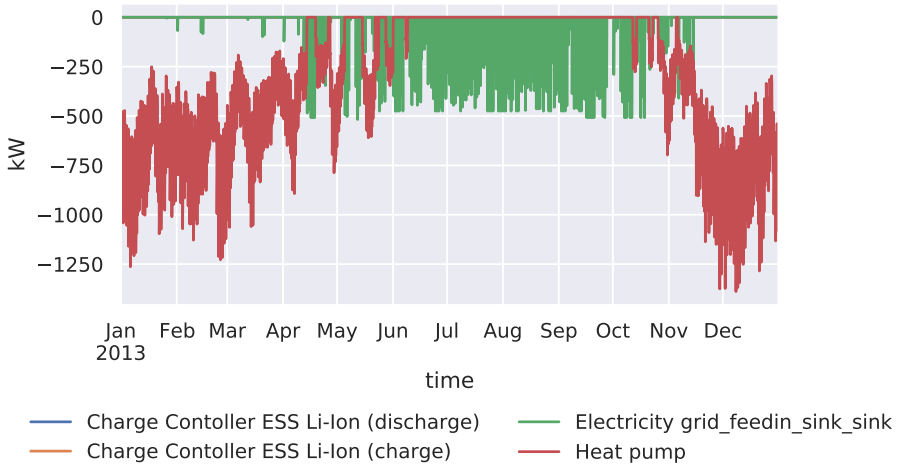

Figure 20: **Charge and discharge flows of ESS Li-ion battery, grid feed-in of electricity and electricity consumption of HP of scenario A2 (in bad weather year in Madrid)**

In order to be more accurate in examining the impact of the sector-coupling by the HP, we additionally compare the sector-coupled scenarios of Madrid (A2, A4 and B2) with a reference scenario of the electricity sector without a Li-ion battery. As shown in figure 21, with the absence of a battery (right), the SC increases in the case of sector coupling compared to the reference scenario (RefE2). On average, it is 9.7 % higher in comparison to RefE2. Feed-in and excess of electricity decrease compared to the reference scenario (RefE2) by 25.3 % and 33.9 % due to a higher internal consumption of the heat pump.

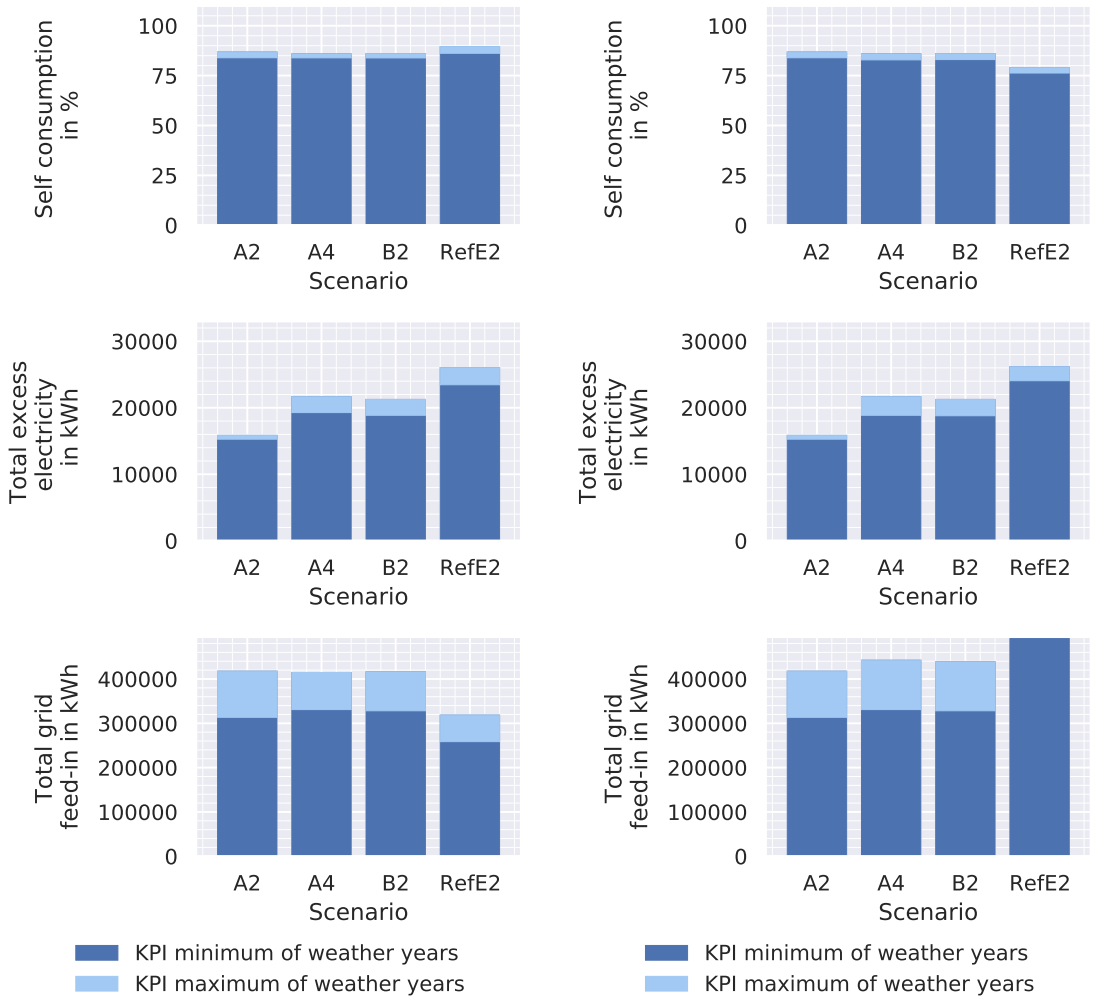

(a) With Li-ion

(b) Without Li-ion

Figure 21: **Self-consumption, total excess electricity and total grid feed-in in the scenarios of Madrid with (a) and without battery (b) with A2: air-to-air HP, A4: air-to-water HP, B2: air-to-water HP with TES and RefE2: reference scenario of electricity sector. The left side of the figure corresponds to the figures 17b and 18b.**

Comparing the two locations Madrid and Berlin we find a higher feed-in and excess of electricity in Madrid when the Li-ion battery is taken out in the simulations (see figure 18a and figure 21b (Without Li-ion)). This is due to higher production of the PV modules connected to higher solar irradiation at this location.

In summary, excess and feed-in decrease in the sector-coupled systems compared to the reference scenario, except for feed-in in Madrid - which increases. Excess and feed-in in the reference scenario in Madrid are at a higher level than in Berlin. With sector-coupling the self-consumption (SC) can be increased by 10.8 % in the case of Berlin and decreases by 2.9 % in the case of Madrid because of the installation of a Li-ion battery in the reference scenario only. There the grid feed-in is reduced significantly and therefore an increase in SC is caused in comparison to the scenarios of sector coupling. If no Li-ion battery is installed, the SC increases by 9.7 % in the case of Madrid in comparison to the reference scenario.

3.4.2. Greenhouse gas emissions of the energy system

Analyzing the total GHG emissions we compare the sector-coupled systems with a reference system that provides the heat supply through a gas boiler. We see according to figure 22, that in the case of Berlin (a) the highest emissions occur in the reference scenario with a gas boiler (RefG1), closely followed by air-to-air HP technology (A1) while the air-to-water HP technology (A3 and B1) shows the least emissions. On average 3.9 % of the total GHG emissions can be saved in the case of sector-coupling with an air-to-air HP (A1), 35.3 % with an air-to-water HP (A3) and 35.3 % with a combination of an air-to-water HP and a TES (B1).

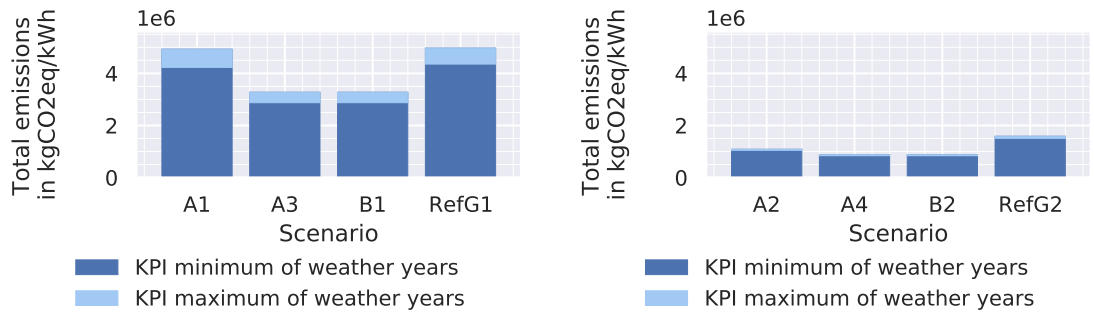

(a) Berlin (b) Madrid

Figure 22: **Total GHG emissions in the scenarios of Berlin (a) and Madrid (b) with A1/A2: air-to-air HP, A3/A4: air-to-water HP, B1/B2: air-to-water HP with TES and RefG1/RefG2: reference with space heating through gas**

In the case of Madrid (b), the total average savings of total GHG emissions due to sector-coupling are higher (40.35 %) than in the case of Berlin (24.9 %). This is due to less total de-

mand in electricity and heat, more PV generation and also a lower emission factor of the grid energy in the case of Spain in comparison to Germany. The combination of an air-to-water HP and a TES (B2) reduces the total GHG emissions by 44.9 % in regard to the reference scenario, closely followed by the air-to-water HP as stand alone (A4), which reduces emissions by 44.9 %. With an air-to-air HP (A2) 31.3 % of total GHG emissions are saved in comparison to the reference scenario (RefG2).

In the case of the sector-coupled systems, the total GHG emissions depend on the amount of the electric energy consumed from the grid, while in the case of the reference scenario with space heating supplied by a gas boiler, total GHG emissions additionally occur due to combustion of natural gas. The total GHG emissions rise with the consumption of electricity. Depending on the heat pump and its coefficient of performance (COP), the consumption of the required electrical energy for the heat pump varies. According to equation 6 a higher quality grade (η) leads to a higher COP with constant temperatures. The COP of an air-to-air HP is, with a quality grade of 0.1852, smaller than the one of the air-to-water HP, to which a quality grade of 0.403 can be assigned. Consequently, more electrical energy is required for the air-to-air technology. In figure 23 the total consumption from the grid is shown for the scenarios of Berlin (a) and Madrid (b). It is striking that, for both locations the air-to-air HP (A1 and A2) has a higher consumption from the grid (in the case of Berlin by 494.6 % on average and in case Madrid by 209.8 % on average in comparison to the reference scenarios (RefG1 and RefG2)).

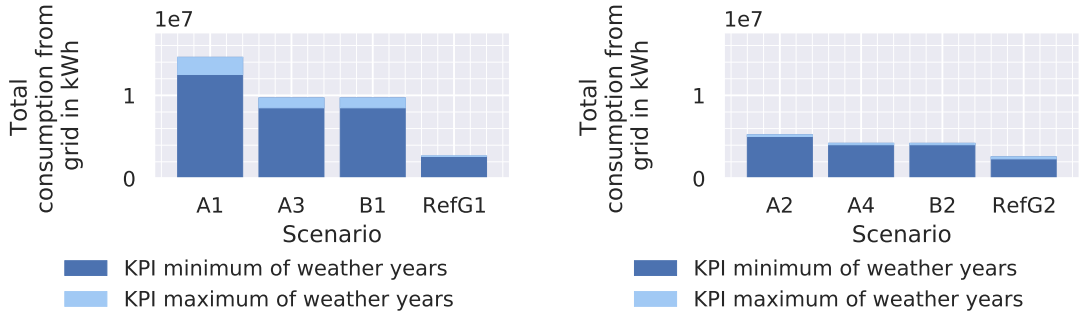

(a) Berlin (b) Madrid

Figure 23: **Total electricity consumption from grid in the scenarios of Berlin (a) and Madrid (b) with A1/A2: air-to-air HP, A3/A4: air-to-water HP, B1/B2: air-to-water HP with TES and RefG1/RefG2: reference scenarios with space heating through gas**

With an air-to-water HP as stand alone (Berlin: A3, Madrid: A4) the total consumption from grid increases compared to the reference scenario by 333.05 % on average in Berlin's scenarios and by 168.5 % on average in the case of Madrid. The total consumption from grid only slightly differs for an air-to-water HP with TES (Berlin: B1 and Madrid: B2) compared to the stand alone technology. Compared to the reference scenario it is increased in the case of Berlin by 333.0 % on average and in the case of Madrid by 168.4 % on average.

3.4.3. Energy system costs

For the cost analysis, we compare all total costs, which are significantly different for each of the sector-coupling scenarios. These are the costs of the HP, the costs of the TES, the costs of the grid consumption, the revenues from the grid feed-in and the costs of the Li-ion battery. The costs of the PV system do not change, since the full capacity is installed in all scenarios. The costs of the solar inverter also diverge only slightly within all scenarios and the two locations and are therefore neglected in the analysis. We further compare the total costs of the energy system of the sector-coupling scenarios with each other and these furthermore with the scenario of heat generation by using natural gas.

Figure 24 shows the total costs of the scenarios in Berlin (a) and Madrid (b). In figure 25 the costs of the grid consumption and feed-in and in figure 26 the costs of the components HP, TES and Li-ion battery are depicted for the scenarios of Berlin (a) and Madrid (b). For Berlin the scenario with an air-to-air HP (A1) shows highest total costs, followed by air-to-water technology, which has slightly lower costs when a TES is installed (B1) than without (A3). Total costs are on average 101.2 % higher in A1 scenario, 57.3 % higher in A3 scenario, and 55.6 % higher in B1 scenario compared to the reference scenario (RefG1). From the comparison of the two figures 25 and 26 it can be further seen that while air-to-air technology is the HP technology with lowest costs, it has the highest costs in terms of grid consumption. The revenues of grid feed-in are similar within the scenarios of sector-coupling (A1, A3 and B1). They are on average 49.2 % lower in comparison to the reference scenario (RefG1). In the scenarios of Berlin (a), only a small capacity of Li-ion battery is installed (approx. 7,500 kWh in RefG1) which is hardly visible in figure 26. This is also only the case for one weather year, where the installation is most favourable regarding the conditions for generating electrical energy from PV.

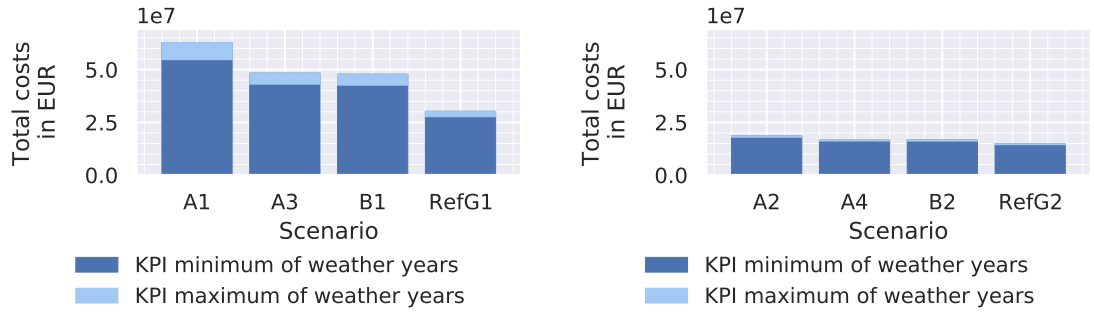

(a) Berlin (b) Madrid

Figure 24: **Total system costs in the scenarios of Berlin (a) and Madrid (b) with A1/A2: air-to-air HP, A3/A4: air-to-water HP, B1/B2: air-to-water HP with TES and RefG1/RefG2: reference scenarios with space heating through gas**

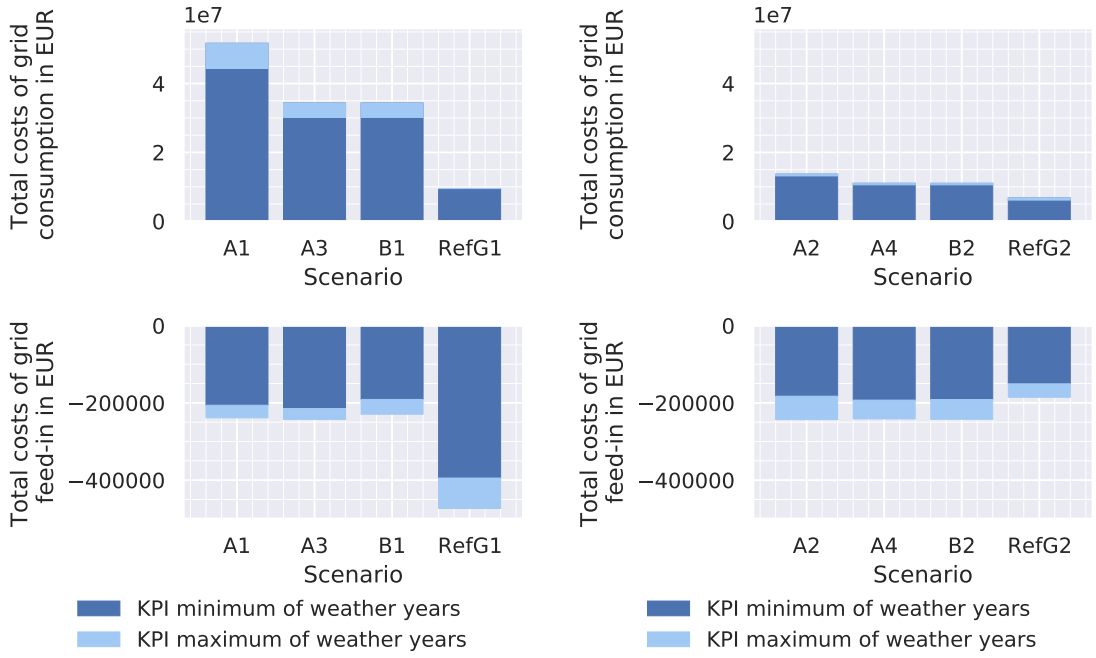

(a) Berlin (b) Madrid

Figure 25: **Total costs of grid consumption and total costs of grid feed-in in the scenarios of Berlin (a) and Madrid (b) with A1/A2: air-to-air HP, A3/A4: air-to-water HP, B1/B2: air-to-water HP with TES and RefG1/RefG2: reference scenarios with space heating through gas**

In Madrid's (b) scenarios as well the air-to-air HP (A2) has the highest costs (24.5 % higher on average than that of the reference scenario (RefG2)) followed by air-to-water HP as stand-alone (12.3 % higher on average than that of RefG2) and by air-to-water HP with TES (12.1 % higher on average than that of RefG2). Also here the costs of grid consumption are in each scenario of sector-coupling (A2, A4 and B2) higher than in the reference scenario (RefG2). However, they are lower compared to the scenarios of Berlin, which is because of a higher PV production and a lower heat demand in Madrid compared to Berlin. As already mentioned, in Madrid there is more grid feed-in in the scenarios of sector-coupling compared to RefG2. For this reason the revenue is also higher (on average 24.8 %). In Madrid's scenarios the Li-ion battery is installed in the case of scenarios containing the air-to-water HP and the reference scenario, whereby significantly more is installed in the reference scenario. From the cost of the battery, it can be deduced that a much higher capacity of the battery is installed compared to the Berlin scenarios.

For Madrid (b) the total costs within all scenarios differ with a standard deviation of 3.1 million EUR less in comparison to Berlin (a), where the standard deviation amounts to 15 million EUR. In Madrid's scenario B2, the costs of the TES relative to the installed heat pump capacity are lower than in Berlin's scenario B1, which results in a smaller difference in costs of the scenarios with the air-to-water HPs. This can be observed comparing the difference

in the HP's total costs ("total costs HP") of A3 and B1 with A4 and B2. In Madrid it is smaller than in Berlin, since in Berlin comparatively more TES capacity is installed. This is due to the higher electricity and heat demand in Berlin compared to Madrid. It is more profitable over the lifetime of the project to install a TES and thus save electrical energy than to purchase it from the grid.

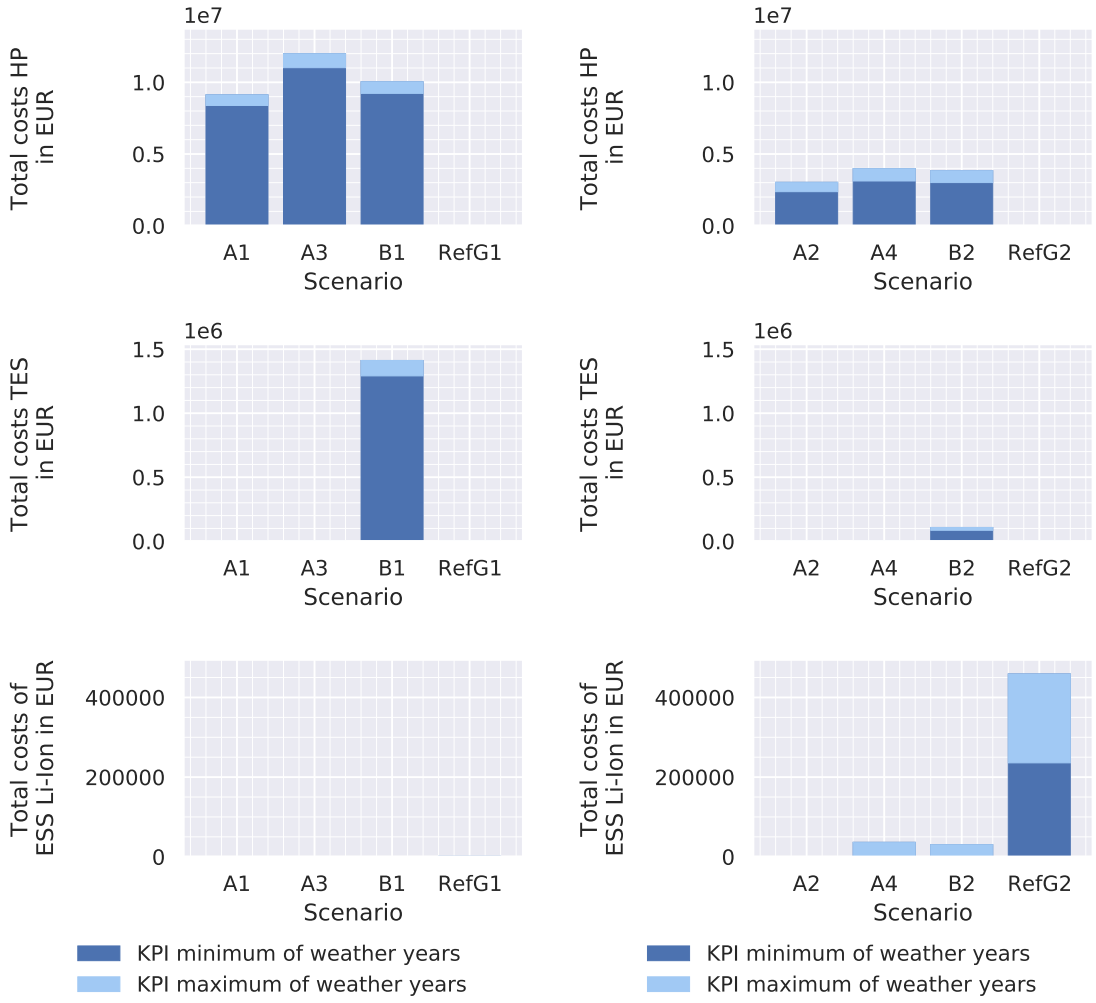

(a) Berlin (b) Madrid

Figure 26: **Total costs of HP, TES and Li-ion battery in the scenarios of Berlin (a) and Madrid (b) with A1/A2: air-to-air HP, A3/A4: air-to-water HP, B1/B2: air-to-water HP with TES and RefG1/RefG2: reference scenarios with space heating through gas**

3.5. Analysis of the sector-coupled energy system with heat pump and thermal energy storage using perovskite-silicon and concentrator PV in comparison to silicon PV as electricity supply

Now we examine the sector-coupled energy system including the new PV technologies CPV and PSI. We compare the KPIs degree of net zero energy (NZE), degree of autonomy (DA), self-consumption (SC), greenhouse gas (GHG) emissions and total system costs of each of the sector-coupled systems with integrated PV technologies SI, CPV and PSI. Here we compare scenarios with the respective state-of-the-art technology for space heating in the examined locations: air-to-water heat pump (HP) including thermal energy storage (TES) in Berlin and air-to-air HP in Madrid.

3.5.1. Degree of net zero energy, degree of autonomy and self-consumption of the energy system

We now analyse the effects of CPV and PSI on sector-coupled scenarios comparing them with the electricity sector regarding the degree of NZE, DA and SC. Figure 27 shows the degree of NZE, the DA and SC for the electricity sector scenarios (*Scenario D* in table 10) and sector-coupled scenarios (*Scenarios B5, C5* and *C7* (Berlin) and *Scenarios A8, C6* and *C8* (Madrid) in table 11) for three PV technologies in Berlin (a) and Madrid (b) and for a varying number of storeys. In all simulations only rooftop applications are considered.

As expected, the SC of the scenarios with sector-coupling is slightly higher compared to the electricity scenarios in both locations, while the degree of NZE and DA is lower. As the general demand is higher in the scenarios with sector-coupling, more of the locally produced electricity can be consumed instantly, without investing in battery storages. However, the higher demand causes a stronger dependency on electricity from the grid, as the production cannot level the high demand. Particularly suitable for illustrating this observation are the scenarios of Madrid with eight storeys. While the SC reaches almost 100 % for SI, the degree of NZE is only at approximately 21 % for the medium weather year. However, it has to be taken into account that only rooftop applications are considered in these scenarios, making the goal to reach NZE unrealistic, also for scenarios of the electricity sector only. The highest degree of NZE of over 80 % for the electricity sector are reached for a three-storey building with SI. In section 3.6 we therefore examine the degree of NZE for installations on rooftop and facades for the maximum installable PV capacity.

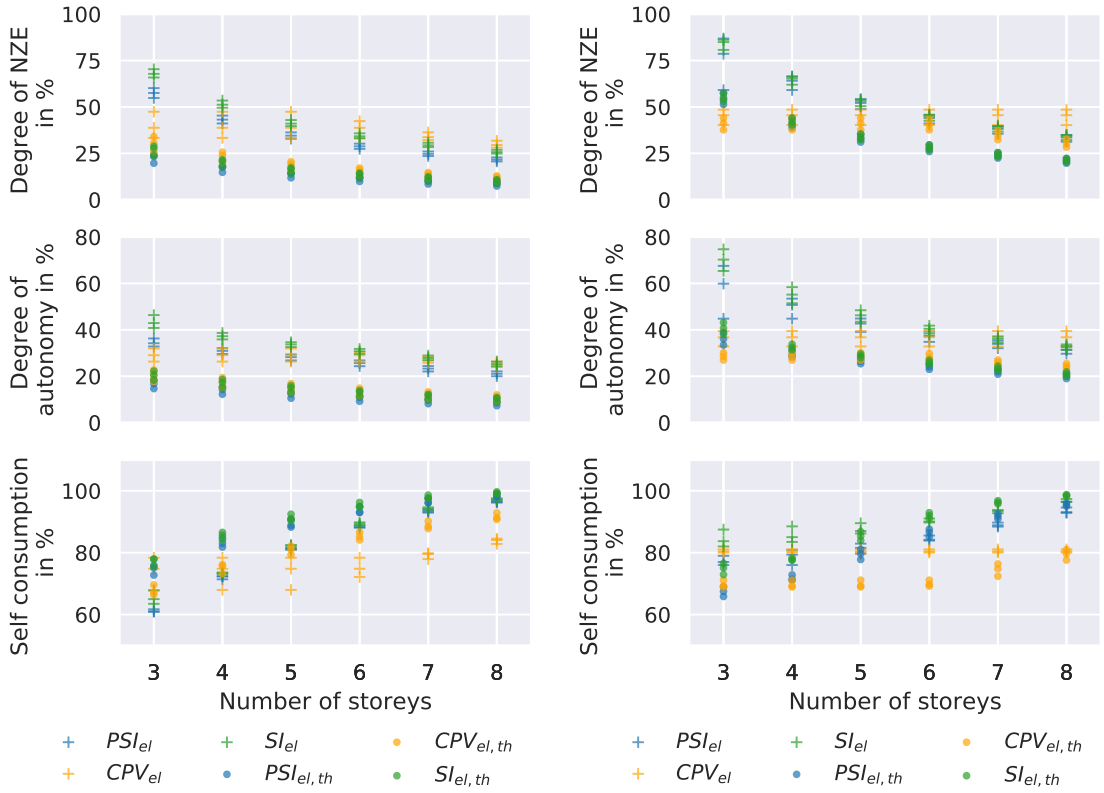

(a) Berlin (b) Madrid

Figure 27: **Degree of NZE, degree of autonomy (DA) and self-consumption (SC) in the electricity sector scenarios (el) and sector-coupled scenarios (el, th) for Berlin (a) and Madrid (b) for three weather years and a varying number of storeys. Only rooftop applications are considered.**

For a more detailed analysis of the SC, we look at KPIs that significantly influence it. For this, we examine the installed PV capacity, the installed capacity of the battery storage and the grid feed-in in the case of sector-coupling and compare these with the electricity sector in the case of a varying number of storeys. In figure 28 the installed capacity of PV and battery storage as well as the total feed-in are shown for Berlin (a) and Madrid (b). While for SI and PSI the maximum PV capacity is installed for all numbers of storeys and both locations, the maximum capacity of CPV is only reached from seven storeys in Berlin and not at all in Madrid in the case of the electricity scenarios. However, in the scenarios of sector-coupling, the maximum capacity is installed from four storeys on in Berlin and from six storeys in Madrid.

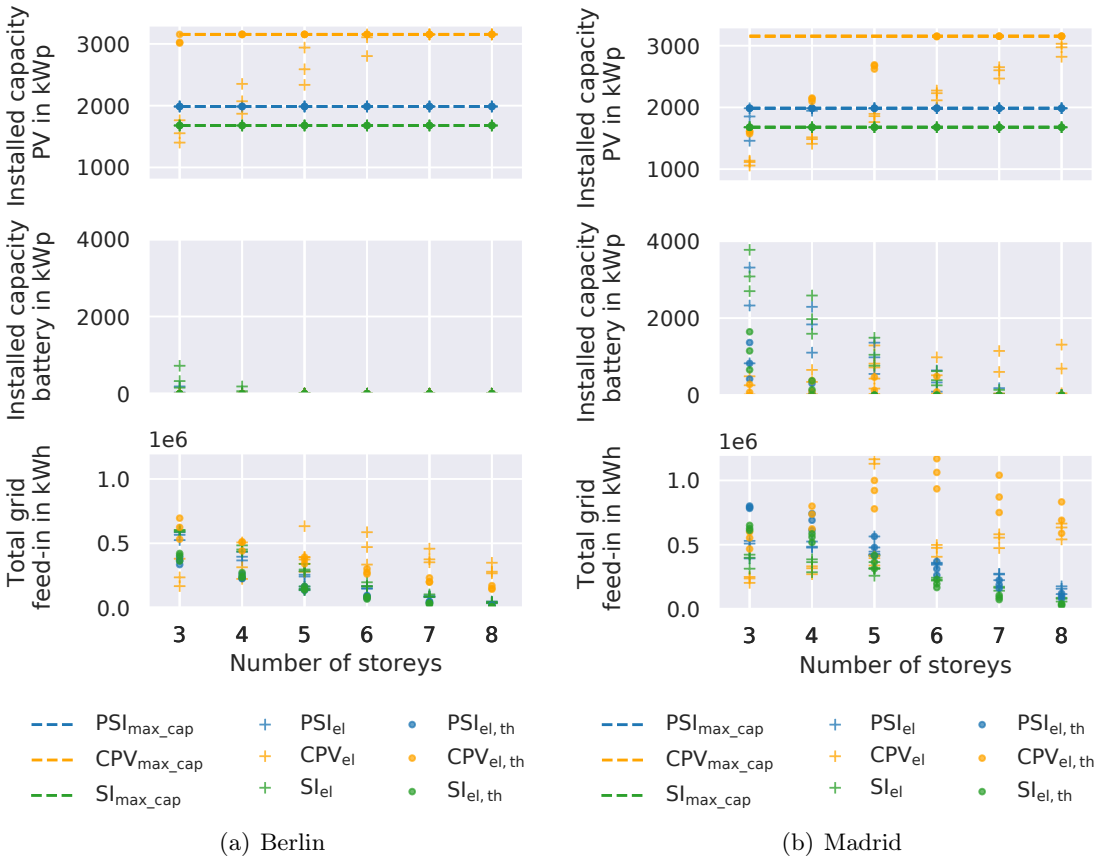

(a) Berlin (b) Madrid

Figure 28: **Installed capacity of PV and battery storage and total grid feed-in in the electricity sector scenarios (el) and sector-coupled scenarios (el, th) for Berlin (a) and Madrid (b) for three weather years and a varying number of storeys. Only rooftop applications are considered.**

In Berlin battery storages are not profitable for scenarios of sector-coupling, because HPs fulfill a similar role like battery storages. In Madrid, only a small capacity is installed in the case of sector-coupling, which decreases as the number of floors and thus the demand increases. But also for the electricity scenarios, battery storages are only profitable for SI and PSI until five to six storeys. In Madrid the battery storage capacities of the electricity scenarios also reduce with the demand, only CPV shows a slight increase with higher storeys.

In the sector-coupling scenario with CPV in the case of Madrid the grid feed-in rises strongly over 1 GWh for six storeys in analogy to the rise in installed capacity. Above number of storeys of more than six, as the maximum installed capacity is reached, the feed-in decreases as the demand increases with the storeys.

Now we study the SC for five storeys comparing the three PV technologies for the sector-coupled case alone. Figure 29 shows the SC in Berlin (a) and Madrid (b) of the scenarios with PSI (Berlin: C1 and Madrid: C2), with CPV (Berlin: C3 and Madrid: C4) and with SI (Berlin: B1 and Madrid: A2) using the state-of-the-art technology of the HP at the respective location

(Berlin: air-to-water HP with TES, Madrid: air-to-air HP). It shows that the highest SC can be found in the scenarios with the basic PV technology: SI (B1 and A2). The use of PSI (C1 and C2) reduces the SC compared to the SI technology by 2.1 % in the case of Berlin and by 6.9 % on average in the case of Madrid. CPV (C3 and C4) further lowers the SC compared to SI by 11.4 % on average for Berlin and by 18.3 % on average in the case of Madrid.

(a) Berlin (b) Madrid

Figure 29: **Self-consumption in the scenarios of Berlin (a) and Madrid (b) with C1: PSI, air-to-water HP with TES, C3: CPV, air-to-water HP with TES, B1: SI, air-to-water HP with TES, C2: PSI, air-to-air HP, C4: CPV, air-to-air HP and A2: SI, air-to-air HP**

The SC depends on the PV production, the excess electricity and the grid feed-in (see section 2.4.2). The total production from PV is shown in figure 30 for Berlin (a) and Madrid (b). In both locations the generation is higher with CPV (17 % in Berlin (C3) and 23.3 % in Madrid (C4) on average) and lower with PSI (15.7 % in Berlin (C1) and 1.1 % in Madrid (C2) on average) compared to SI. The larger percentage difference in PV production of CPV versus SI is due to the fact that a higher capacity of CPV can be installed due to the smaller module size, while the efficiency of CPV is higher. As described in section 3.1.1, the production per m^2 is lowest for SI and highest for CPV in both locations (see figure 5). The effect can further be observed in figure 28, where the installed capacity of PV is shown for Berlin (a) and Madrid (b). The installed capacity is higher in the case of CPV in comparison to SI for a five-storey building and both locations. In the case of PSI more capacity is installed but less electricity is generated in both locations (see figure 30 (C1 and C2) and figure 28).

In figure 31 the total excess electricity and the total grid feed-in are depicted for Berlin (a) and Madrid (b). It should be noted that the excess electrical energy is two orders of magnitude smaller than the grid feed-in. The electricity excess is lowest for the SI technology (B1 and A2). With PSI (C1 and C2) the electricity excess increases by 83.2 % in Berlin and 172.2 % in Madrid on average compared to SI. We would have expected a decrease in the excess, since the production in the case of PSI is on average lower than that of SI. We further observe that the consumption from the grid is higher in the case of PSI in comparison to SI on average by about 268 MWh in Berlin and about by 173 MWh in Madrid.

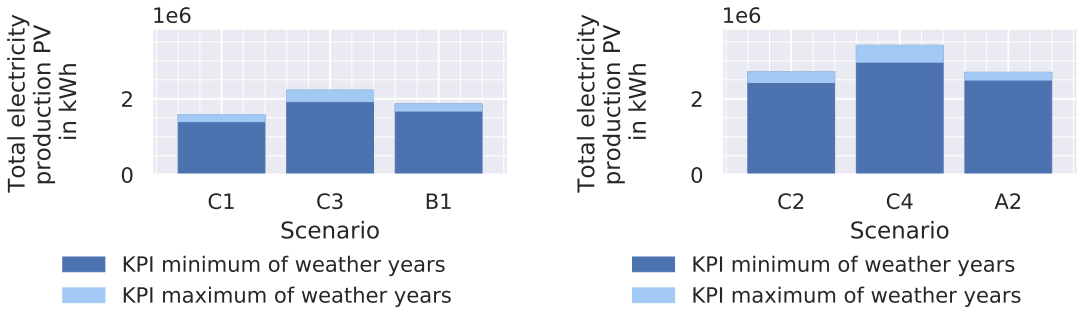

(a) Berlin (b) Madrid

Figure 30: **Total electricity production of PV in the scenarios of Berlin (a) and Madrid (b) with C1: PSI, air-to-water HP with TES, C3: CPV, air-to-water HP with TES, B1: SI, air-to-water HP with TES, C2: PSI, air-to-air HP, C4: CPV, air-to-air HP and A2: SI, air-to-air HP**

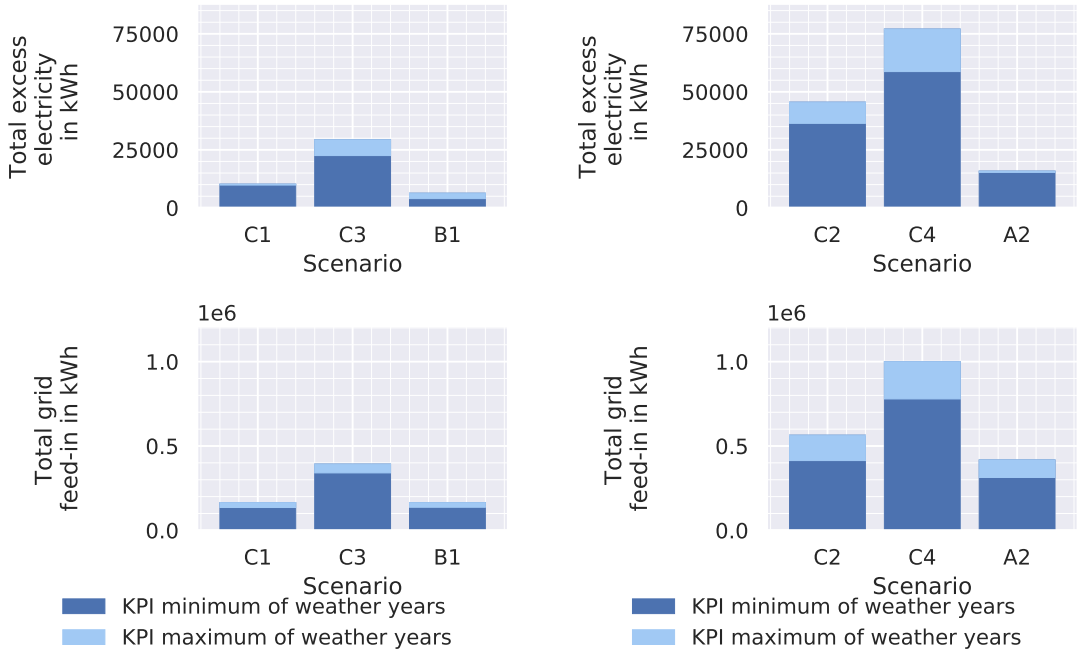

(a) Berlin (b) Madrid

Figure 31: **Total excess electricity and total grid feed-in of the scenarios in Berlin (a) and Madrid (b) with C1: PSI, air-to-water HP with TES, C3: CPV, air-to-water HP with TES, B1: SI, air-to-water HP with TES, C2: PSI, air-to-air HP, C4: CPV, air-to-air HP and A2: SI, air-to-air HP**

Using CPV the excess increases by 367 % in Berlin and 347.9 % in Madrid on average, due to higher PV production. Here the consumption from the grid is higher in the case of Madrid by about 19 MWh and lower in the case of Berlin by about 45 MWh.

In Berlin (a) the feed-in increases in the case of CPV by 148.3 %. In the case of PSI it is approximately equal (0.01 % lower compared to SI). In Madrid (b) the feed-in increases in the case of PSI by 32.9 % and in the case of CPV by 146.4 %. For CPV, the increase is in line with our expectations as more PV power is generated and thus more feed-in occurs for the same demand. However, for the comparatively high feed-in in the case of CPV, the type of solar irradiance is crucial. Due to the fact that it is strongly dependent on DNI radiation, the daily profile of generated power is narrower than in the case of SI. The dependence on the type of irradiance is even more evident in the case of PSI. Although less PV power is generated on average, the total annual grid consumption and grid feed-in is larger than for SI. This is because more PV power is generated in the middle of the day with PSI than with SI, where at the same time the demand is comparatively low. As a consequence the feed-in rises at this time of the day. This is illustrated in Figure 32. There, the output of the solar inverter, the power fed into the grid, and the demand of electric power are shown under SI (left) and PSI (right) are shown as an example for calendar week 28 of 2013. This could also be the explanation why the excess is higher with PSI than with SI, contrary to our expectations: Excess electrical DC power of the PV modules, which occurs when the midday peak is higher than the solar inverter's capacitiy a is not converted into AC power.

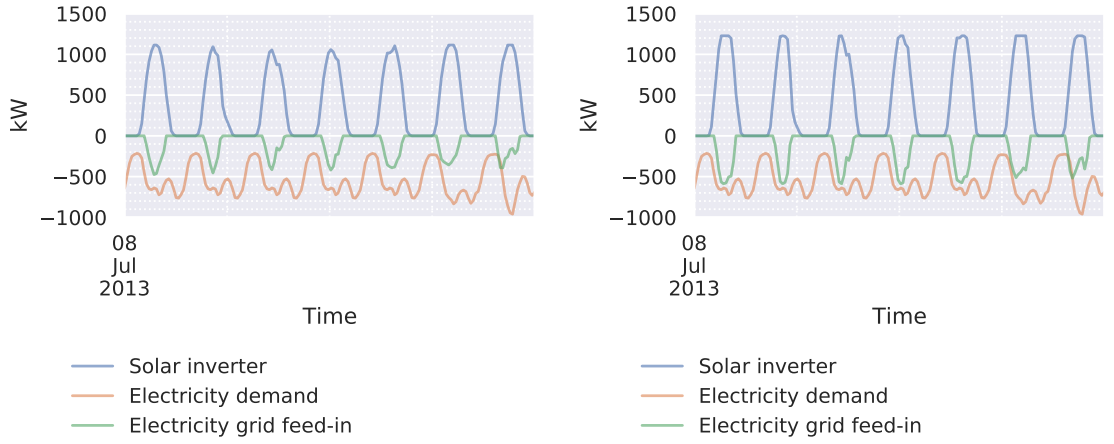

(a) SI (A2)

(b) PSI (C2)

Figure 32: **Electricity output of solar inverter, grid feed-in of electricity and electricity demand in the 28th calendar week of 2013 of SI (a) and PSI (b)**

3.5.2. Greenhouse gas emissions of the energy system

All three energy systems with different PV technologies have similar emissions at the respective location (see figure 33). With the usage of PSI (C1 and C2) the emissions increase by 3 % on average in the scenarios of Berlin and 3.4 % on average in the scenarios of Madrid compared to the SI technology. They slightly decrease using CPV technology in Berlin by 0.5 % and increase in the case of Madrid by 0.4 % on average. This small variance in GHG emissions is explained by similar grid consumption across the scenarios (see figure 34).

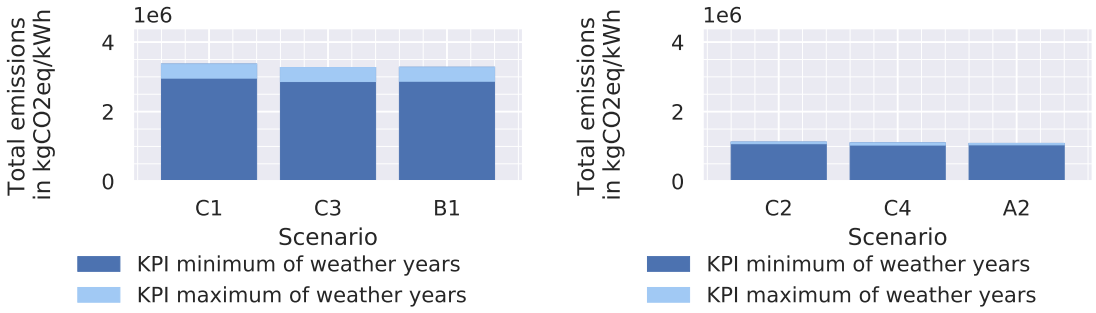

(a) Berlin (b) Madrid

Figure 33: **GHG emissions in the scenarios of Berlin (a) and Madrid (b) with C1: PSI, air-to-water HP with TES, C3: CPV, air-to-water HP with TES, B1: SI, air-to-water HP with TES, C2: PSI, air-to-air HP, C4: CPV, air-to-air HP and A2: SI, air-to-air HP**

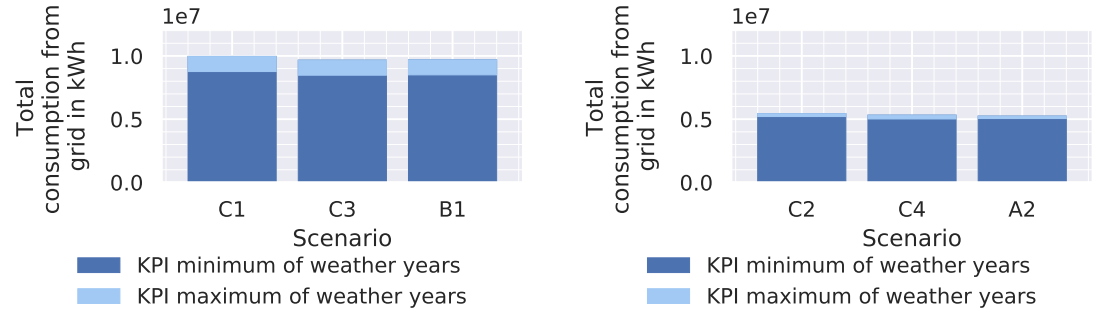

(a) Berlin (b) Madrid

Figure 34: **Total grid consumption in the scenarios of Berlin (a) and Madrid (b) with C1: PSI, air-to-water HP with TES, C3: CPV, air-to-water HP with TES, B1: SI, air-to-water HP with TES, C2: PSI, air-to-air HP, C4: CPV, air-to-air HP and A2: SI, air-to-air HP**

3.5.3. Energy system costs

Total costs do not vary over scenarios of Berlin and Madrid in a significant way (see figure 35). For Berlin the costs rise with PSI (C1) by 2.3 % and with CPV (C3) by 3.3 % in comparison to SI (B1). In the case of Madrid, the costs increase by 2.52,% with PSI (C2) and by 6.3 % with CPV (C4) compared to SI (A2). Also the total costs of HP, TES, grid consumption do not vary significantly over the examined scenarios of both locations, so they are not further discussed. The revenue by feed-in, which is depicted in figure 36 is higher for both locations in the case of PSI and CPV, which is mainly compensated by higher solar inverter costs. For the solar inverter, a higher capacity is installed due to the higher PV production of PSI and CPV compared to SI (see figure 30).

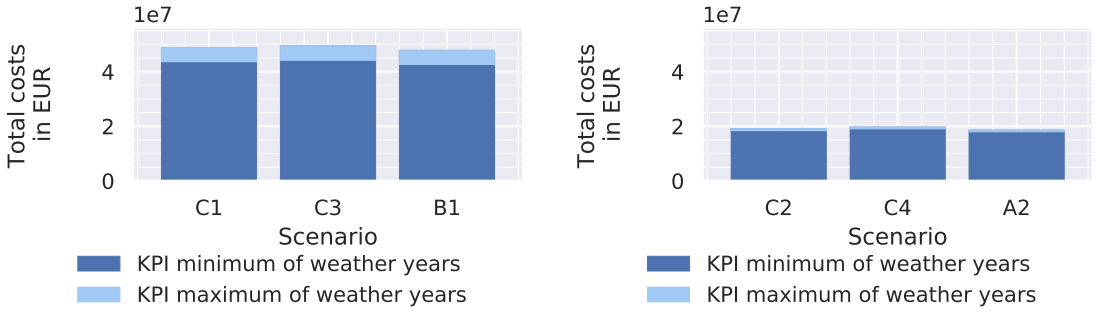

(a) Berlin (b) Madrid

Figure 35: **Total system costs in the scenarios of Berlin (a) and Madrid (b) with C1: PSI, air-to-water HP with TES, C3: CPV, air-to-water HP with TES, B1: SI, air-to-water HP with TES, C2: PSI, air-to-air HP, C4: CPV, air-to-air HP and A2: SI, air-to-air HP**

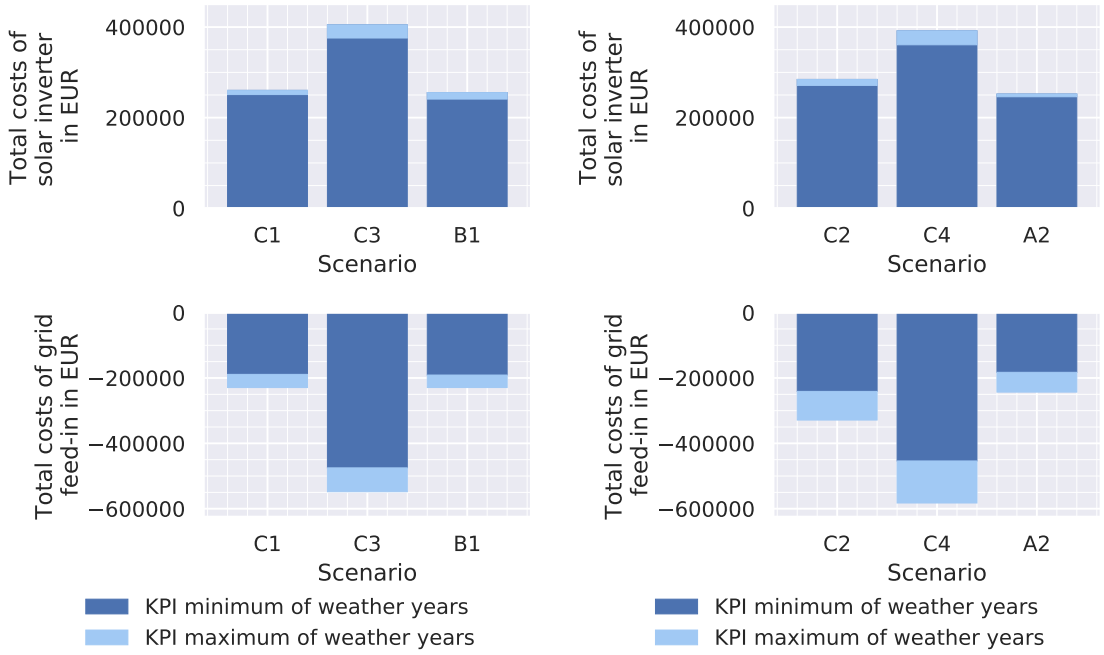

(a) Berlin (b) Madrid

Figure 36: **Total costs of solar inverter and total costs of grid feed-in in the scenarios of Berlin (a) and Madrid (b) with C1: PSI, air-to-water HP with TES, C3: CPV, air-to-water HP with TES, B1: SI, air-to-water HP with TES, C2: PSI, air-to-air HP, C4: CPV, air-to-air HP and A2: SI, air-to-air HP**

3.6. Potential of concentrator and perovskite-silicon PV for supplying the sector-coupled energy system as net zero energy communities, in comparison to silicon PV

After having analysed different KPIs we examine the potential for supplying the demand of the sector-coupled system as NZE community. In these scenarios the maximum capacity of PV (rooftop as well as facades) and the respective state-of-the-art technology for space heating are installed. In figure 37 the degree of NZE as well as the DA and the SC are depicted for sector-coupled scenarios with SI, PSI and CPV in Berlin (a) and Madrid (b) over a varying number of storeys. In Berlin, none of the three PV technologies reaches NZE status in all three weather years. For single-storey buildings, the degree of NZE is comparatively high with up to 72.4 % with PSI, up to 99.9 % with CPV, and up to 84.1 % with SI. With higher number of storeys and thus higher demand, the degree of NZE decreases and remains approximately constant above a number of three storeys at values between 19.4 and 24.3 % with PSI, 26.8 and 34.0 % with CPV and 24.4 and 30.8 % with SI. In the case of single-storey buildings the degree of NZE is reached in Madrid (b) with all PV technologies and above that for two-storey buildings with CPV only. For single-storey buildings, the degree of NZE takes a value up to 170.5 % with PSI, up to 255.6 % with CPV, and up to 170.9 % with SI. The degree of NZE decreases with higher number of storeys and varies from 50.3 and 57.0 % with PSI, 68.4 and 80.4 % with CPV, and 54.3 and 59.9 % with SI above three storeys. In Madrid, the CPV technology has a higher degree of NZE compared to the other two technologies, where the degree of NZE is approximately the same. In Berlin, the range of the degree of NZE of the technologies is smaller than in Madrid. This is due to the fact that there is more installed capacity of CPV in comparison to the other technologies and at the same time, in the case of Madrid, more feed-in with approximately similar grid consumption over all PV technologies. To illustrate these relations, the grid feed and the consumption from the grid are shown together with the installed PV capacity in figure 38 for Berlin (a) and Madrid (b).

When examining the DA, figure 37 shows that it also decreases with increasing demand. Above three storeys it is comparatively constant and varies in the case of all PV technologies between 14.8 and 24.9 % in Berlin (a) and between 34.1 and 54.8 % in Madrid (b).

The SC increases from a number of one to three storeys, since less grid feed-in takes place with approximately the same installed capacity of PV as can be seen in figure 38. From a number of three storeys on, the SC varies approximately constantly around the values between 68.5 and 79.4 % in the case of Berlin and around values between 66.0 and 80.1 % in the case of Madrid considering all PV technologies. From this it can be deduced that the generation from PV increases together with feed-in and excess electricity in nearly the same proportion.

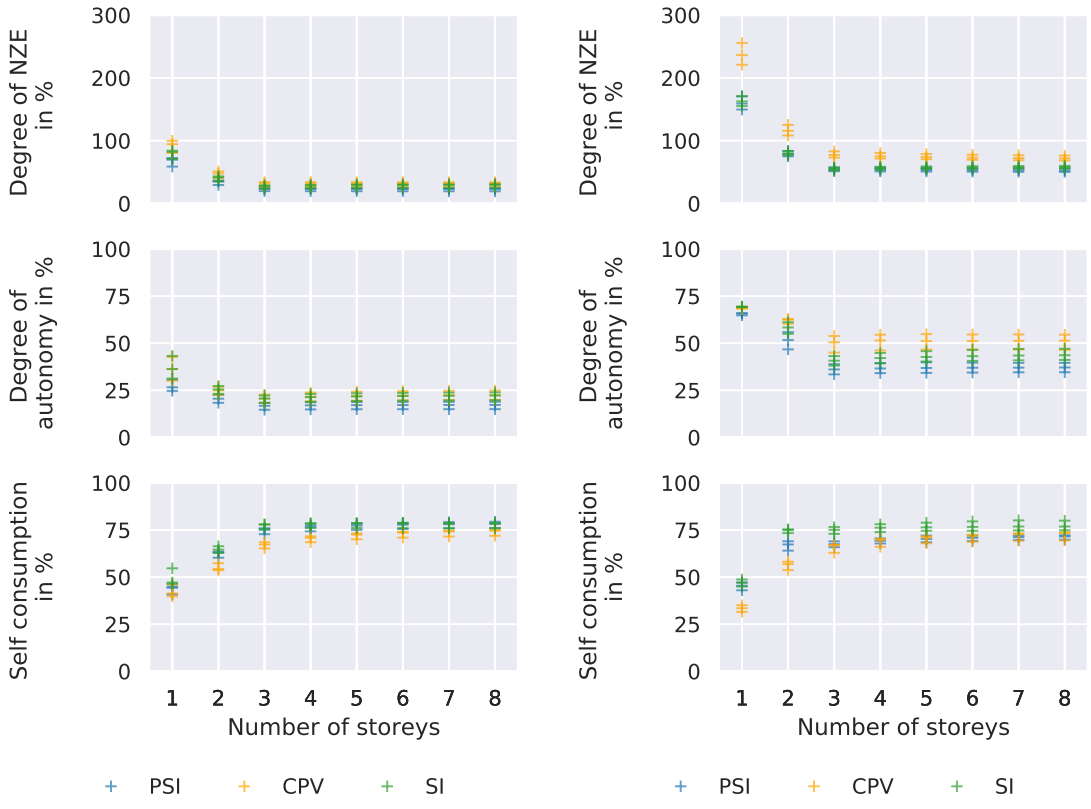

(a) Berlin (b) Madrid

Figure 37: **Degree of NZE, degree of autonomy (DA) and self-consumption (SC) with three PV technologies for sector-coupled systems in Berlin (a) and Madrid (b) for varying number of storeys and three years, taking a flat roof and three facades (south, east and west) into account**

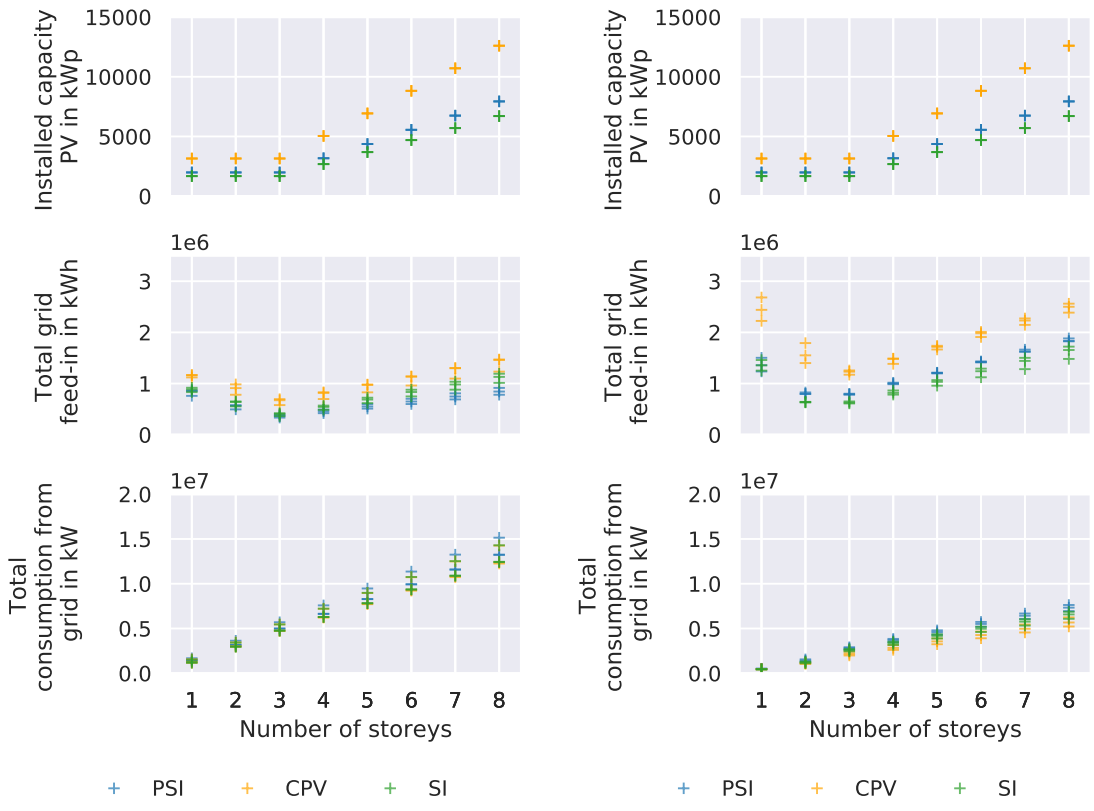

(a) Berlin

(b) Madrid

Figure 38: **Installed PV capacity, total grid feed-in and total consumption from grid with three PV technologies for sector-coupled systems in Berlin (a) and Madrid (b) for varying number of storeys and three years, taking a flat roof and three facades (south, east and west) into account**

4. Conclusion

This work examines the influence of three innovative photovoltaic (PV) technologies onto urban residential energy systems. We analyse hybrid high concentrator photovoltaics (HCPV) silicon modules, further called concentrator photovoltaics (CPV), fictitious high efficient tandem perovskite-silicon (PSI) modules, and PV-powered heat pumps (HPs) in an energy system analysis in comparison to state-of-the-art technologies: multi-crystalline silicon (SI) PV and heat supply by a gas boiler. In this context, we examine the influence on degree of autonomy (DA), self-consumption (SC), total system costs and greenhouse gas (GHG) emissions of the energy system in an energy system analysis with linear optimisation. Additionally, we explore the potential for supplying net zero energy (NZE) communities with these technologies, meeting the criteria that energy consumed from the grid should not exceed the energy that is fed into the grid during the period of one year. We focus on the local energy system of fictional residential areas of 20 buildings under two different climatic conditions in Madrid, Spain, and Berlin, Germany. As especially CPV is highly dependent on the direct irradiance, we further examine the influence of the location and grid parameters, such as energy prices and feed-in tariff in ten additional European locations.

Our main findings are clustered per technology stating the sections, where the respective results can be found in detail.

Concentrator photovoltaics (CPV)

- The space saving CPV reaches higher energy yields per m^2 than SI and PSI in both locations, while the yield is greatest in Madrid. Due to its lower performance ratio (PR), CPV has the highest LCOE and lowest energy yield per kWp of the analysed technologies. (Section 3.1.1)

- In order to compete with SI under current regulations, the specific investment costs of CPV would have to be reduced. To reach a comparable LCOE, the specific investment costs should be lowered to around 550 EUR/kWp in Berlin and around 750 EUR/kWp in Madrid. Comparing the technologies on a system level, the costs would have to be reduced further in order to reach similar total system costs (500 EUR/kWp in Berlin and 600 EUR/kWp in Madrid). The specific investment costs may be higher for use cases that require a high degree of autonomy or degree of NZE. (Section 3.1.3)

- When requiring a NZE community, the advantage of the space saving CPV technology becomes clear: In the electricity sector scenarios for PSI, only single-storey buildings in Berlin and two-storey buildings in Madrid allow for a NZE community. SI allows two-storey buildings to be realised in both locations. In contrast, CPV allows for two storeys in Berlin and up to eight storeys in Madrid. This NZE configuration for CPV requires 21 % higher system costs than the cost-optimal solution without requiring

NZE. In these scenarios, rooftop installations as well as facades from the third storey on are taken into account. In areas where space is an issue and where facades might not be available for PV installations, e.g. due to shading, CPV allows for the maximum yield of production. (Section 3.2.2)

- Also in the sector-coupled scenarios with state-of-the-art space heating at the respective location (Berlin: air-to-water HP with thermal energy storage (TES), Madrid: air-to-air HP), the space saving characteristic of CPV allows for a NZE community in Madrid for up to two-storey buildings with PV installations on rooftops, while SI and PSI only supply single-storey buildings as an NZE community. In Berlin, a NZE community is almost reached for single-storey buildings when the maximum installable capacity on rooftops is employed (degree of NZE: 99.9 %). (Section 3.6)

- Analyzing the effects of the technologies on costs and emissions of the energy system on a European level has shown that CPV with its high specific investment costs is more likely to be profitable in locations with high direct normal irradiance. Due to the high specific investment costs, CPV is not profitable in countries with low electricity prices and/or low feed-in tariffs.

Perovskite-silicon (PSI) technology

- The energy yield per m^2 of the low-cost technology PSI exceeds the energy yield of SI, but is lower than the one of CPV. Even though PSI has lower specific investment as well as operation and maintenance costs, its LCOE is higher than the one of SI. The lower PR of PSI leads to more kWp having to be installed to produce the same amount of kWh. (Section 3.1.1)

- The sensitivity analysis of the lifetime and specific investment costs of PSI has shown that lower lifetimes are acceptable, when costs are reduced significantly. At low specific investment costs of 500 EUR/kWp, a lifetime of 12 years in Madrid and a lifetime of 18 years in Berlin achieves a LCOE comparable to SI. Comparing the technologies on system level, PSI is only reaching total system costs comparable to SI for long lifetimes (25 years) and low specific investment costs of around 500 EUR/kWp. (Section 3.1.2)

- In the scenarios with electricity only, a comparatively small increase of the total system costs of less than 10 % would have a great effect on the facilitation of nearly zero energy building (nZEB) communities with PSI, almost reaching NZE in the location of Madrid (degree of NZE of 82 % for eight-storey buildings). In Berlin, a degree of NZE of 57 % can be reached for eight storeys. However, SI reaches a higher degree of NZE than PSI at lower costs. If costs of PSI can be reduced they might be a good alternative for SI. (Section 3.2.2)

- In the sector-coupled energy system with state-of-the-art space heating at the respective location (Berlin: air-to-water HP with TES, Madrid: air-to-air HP) with PSI as well as with SI, only single-storey buildings can be supplied as an NZE community in Madrid. SI reaches a slightly higher degree of NZE for two-storey buildings than PSI. (Section 3.6)

Sector-coupling with PV-powered heat pumps (HPs) and thermal energy storage (TES)

- In general, scenarios with sector-coupling show lower degrees of NZE, higher dependency on the grid, but higher SC in comparison to the reference scenario with electricity only (only rooftop applications considered). By coupling the electricity and heat sector with heat pumps, the SC of the energy system can be increased by 10.8 % in the case of Berlin and decreases by 2.9 % in the case of Madrid, due to the installation of a Li-ion battery in the reference scenario only. If no Li-ion battery is installed, the SC increases by 9.7 % in the case of Madrid in comparison to the reference scenario. (Sections 3.4.1 and 3.5.1)

- Compared to the reference scenario of the uncoupled system heat supply by gas, the GHG emissions of the sector-coupled system decrease by a mean of 24.9 % in Berlin and by a mean of 40.4 % in Madrid. The sector-coupled system has higher costs on average, compared to the reference scenario with heat supply by gas. In the case of Berlin, it increases by an average of 71.4 % and in Madrid by an average of 16.3 %. (Sections 3.4.2 and 3.4.3)

- In the sector-coupled systems, no battery is installed in Berlin. In Madrid, only small battery capacities are installed compared to the electricity-only sector, with decreasing battery capacity as the number of storeys increases. This is because batteries are only profitable in scenarios of lower demand (which corresponds to a lower number of storeys) and where no HPs are installed as they reduce, if not zero out, the grid feed-in during periods of their operation, and therefore take on the role of electrical storage. (Section 3.4.1 and 3.5.1)

- With a TES, the total costs of the sector-coupled system can be slightly reduced in Berlin and Madrid. Advantages in terms of self-consumption are only marginally evident in the case of Berlin, where a higher TES capacity is installed compared to Madrid. In Berlin, the TES slightly reduces the feed-in into the electricity grid, resulting in a slightly higher self-consumption than in the stand-alone case of the HP. (Section 3.4.3 and 3.4.1)

To conclude, we have extensively studied the three technologies CPV, PSI, and PV-powered HPs in different energy supply scenarios. We have found that under current regulations, specific investment costs of CPV and PSI would have to be lowered in order to compete with the SI technology. However, the use case of NZE communities shows the advantage of the space saving technology CPV. The PSI technology is positioned between CPV and

SI in terms of efficiency and specific investment costs. With our assumptions regarding efficiency and costs of PSI, we found no plausible advantage over SI in the calculated scenarios. It is to be investigated whether with lower specific investment costs PSI would be a good alternative to silicon and whether with a higher efficiency it would replace CPV in the use case of NZE communities. We have further demonstrated that PV-powered HPs are an appropriate technology for increasing the SC and lowering the GHG emissions of an energy system.

The effect of these technologies on energy systems should be further explored. Especially as PSI is on a low technological readiness level (TRL), there is a comparably high uncertainty in the assumptions of the PSI model, which can be reduced when the TRL is increased.

References

Energinet, D. E. A.
bibinitperiod. (2016). Technology Data for heating installations. Retrieved 12/03/2020, from https://ens.dk/sites/ens.dk/files/Analyser/technology_data_catalogue_for_individual_heating_installations.pdf

Energinet, D. E. A.
bibinitperiod. (2018). Technology Data Energy storage. Retrieved 12/03/2020, from https://ens.dk/sites/ens.dk/files/Analyser/technology_data_catalogue_for_energy_storage.pdf

Askins, S., Jost, N., Aguilar, A. F., Anglade, L., Nardin, G., Duchemin, M., ... Anton, I. (2019). Performance of Hybrid Micro-Concentrator Module with Integrated Planar Tracking and Diffuse Light Collection. In 2019 IEEE 46th Photovoltaic Specialists Conference (PVSC) (pp. 2507–2512). Chicago,USA. doi:10.1109/PVSC40753.2019.8980519

Askins, S., Nardin, G., Ackermann, M., Gerlich, F., & Dominguez, C. (2019). Outdoor monitoring of a hybrid micro-CPV solar panel with integrated micro-tracking and diffuse capture. Version v1.0. Zenodo. doi:https://doi.org/10.5281/zenodo.3346823

Battaglia, M., Haberl, R., Bamberger, E., & Haller, M. (2017). Increased self-consumption and grid flexibility of PV and heat pump systems with thermal and electrical storage. Energy Procedia, 135, 358–366. doi:10.1016/j.egypro.2017.09.527

Beck, T., Kondziella, H., Huard, G., & Bruckner, T. (2017a). Optimal operation, configuration and sizing of generation and storage technologies for residential heat pump systems in the spotlight of self-consumption of photovoltaic electricity. Applied Energy, 188, 604–619. doi:10.1016/j.apenergy.2016.12.041

Beck, T., Kondziella, H., Huard, G., & Bruckner, T. (2017b). Optimal operation, configuration and sizing of generation and storage technologies for residential heat pump systems in the spotlight of self-consumption of photovoltaic electricity. Applied Energy, 188, 604–619. doi:10.1016/j.apenergy.2016.12.041

Ben Youssef, W., Maatallah, T., Menezo, C., & Ben Nasrallah, S. (2018). Assessment viability of a concentrating photovoltaic/thermal-energy cogeneration system (CPV/T) with storage for a textile industry application. Solar Energy, 159, 841–851. doi:10.1016/j.solener.2017.11.058

Bhat, A., Dhamaniya, B. P., Chhillar, P., Korukonda, T. B., Rawat, G., & Pathak, S. K. (2018). Analysing the Prospects of Perovskite Solar Cells within the Purview of Recent Scientific Advancements. Crystals, 8(6). doi:10.3390/cryst8060242

Brandoni, C., Renzi, M., Caresana, F., & Polonara, F. (2014). Simulation of hybrid renewable microgeneration systems for variable electricity prices. Applied Thermal Engineering, 71(2), 667–676. doi:10.1016/j.applthermaleng.2013.10.044

Burhan, M., Chua, K. J. E., & Ng, K. C. (2016). Sunlight to hydrogen conversion: Design optimization and energy management of concentrated photovoltaic (CPV-Hydrogen)

system using micro genetic algorithm. Energy, 99, 115–128. doi:10.1016/j.energy.2016.01.048

Burhan, M., Shahzad, M. W., & Ng, K. C. (2017). Development of performance model and optimization strategy for standalone operation of CPV-hydrogen system utilizing multi-junction solar cell. International Journal of Hydrogen Energy, 42(43), 26789–26803. doi:10.1016/j.ijhydene.2017.08.186

Carlisle, N., Geet, O. V., & Pless, S. (2009). Definition of a 'Zero Net Energy' Community. National Renewable Energy Laboratory. Colorado.

Chang, N. L., Ho-Baillie, A., Vak, D., Gao, M., Green, M., & Egan, R. (2018). Manufacturing cost and market potential analysis of demonstrated roll-to-roll perovskite photovoltaic cell processes. Solar Energy Materials and Solar Cells, 174, 314–324. doi:10.1016/j.solmat.2017.08.038

Chen, B., Baek, S.-W., Hou, Y., Aydin, E., De Bastiani, M., Scheffel, B., ... Sargent, E. (2020). Enhanced optical path and electron diffusion length enable high-efficiency perovskite tandems. Nature Communications, 11(1). doi:10.1038/s41467-020-15077-3

Cole, R. J. & Fedoruk, L. (2015). Shifting from net-zero to net-positive energy buildings. Building Research and Information, 43, 111–120. doi:10.1080/09613218.2014.950452

DAgostino, D., Mele, L., Minichiello, F., & Renno, C. (2020). The Use of Ground Source Heat Pump to Achieve a Net Zero Energy Building. Energies, 13(13). doi:10.3390/en13133450

dos Santos, Í. P. & Rüther, R. (2012). The potential of building-integrated (BIPV) and building-applied photovoltaics (BAPV) in single-family, urban residences at low latitudes in Brazil. Energy and Buildings, 50, 290–297. doi:10.1016/j.enbuild.2012.03.052

ECMWF. (n.d.). ERA5. Accessed: 2010-09-30. Retrieved from https://www.ecmwf.int/en/forecasts/datasets/reanalysis-datasets/era5

EEA, the European Environment Agency. (2021). Greenhouse gas emission intensity of electricity generation in Europe Figure 2. Retrieved 02/21/2021, from https://www.eea.europa.eu/data-and-maps/indicators/overview-of-the-electricity-production-3/assessment

Enerdata. (n.d.-a). Electricity consumption of households for water heating. Retrieved 02/17/2021, from https://odyssee.enerdata.net/database/

Enerdata. (n.d.-b). Electricity consumption of residential for cooking. Retrieved 02/17/2021, from https://odyssee.enerdata.net/database/

Enerdata. (n.d.-c). Electricity consumption of residential for space heating. Retrieved 02/17/2021, from https://odyssee.enerdata.net/database/

Enerdata. (n.d.-d). Electricity consumption of residential sector. Retrieved 02/17/2021, from https://odyssee.enerdata.net/database/

Enerdata. (n.d.-e). Final consumption of residential for cooking. Retrieved 02/17/2021, from https://odyssee.enerdata.net/database/

Enerdata. (n.d.-f). Final consumption of residential for space heating. Retrieved 02/17/2021, from https://odyssee.enerdata.net/database/

European Commission. (2020). Heating and cooling. Retrieved 09/19/2020, from https://ec.europa.eu/energy/topics/energy-efficiency/heating-and-cooling_en

Eurostat, the Statistical Office of the European Union. (n.d.-a). Electricity prices by type of user. Retrieved 04/16/2021, from https://ec.europa.eu/eurostat/databrowser/view/ten00117/default/table?lang=en

Eurostat, the Statistical Office of the European Union. (n.d.-b). Population on 1 January by age, sex and broad group of citizenship. Retrieved 05/05/2021, from https://ec.europa.eu/eurostat/databrowser/view/migr_pop2ctz/default/table?lang=en

Fraunhofer ISE. (2015). Current and Future Cost of Photovoltaics. Long-term Scenarios for Market Development, System Prices and LCOE of Utility-Scale PV Systems. Study on behalf of Agora Energiewende.

Gerstmaier, T., Gómez Padrón, M. G., Gombert, A., Mermoud, A., & Lejeune, T. (2011). Validation of the PVSyst Performance Model for the Concentrix CPV Technology. AIP Conference Proceedings, 1407, 366–369. doi:10.1063/1.3658363

Good, C., Kristjansdottír, T., Houlihan Wiberg, A., Georges, L., & Hestnes, A. G. (2016). Influence of PV technology and system design on the emission balance of a net zero emission building concept. Solar Energy, 130, 89–100. doi:10.1016/j.solener.2016.01.038

Green, M. A., Dunlop, E. D., Levi, D. H., Hohl-Ebinger, J., Yoshita, M., & Ho-Baillie, A. W. Y. (2019). Solar Cell Efficiency Tables (Version 54). 27(7). doi:10.1002/pip.3171

Hachem, C., Athienitis, A., & Fazio, P. (2014). Energy performance enhancement in multistory residential buildings. Applied Energy, 116, F9–19. doi:10.1016/j.apenergy.2013.11.018

Hao, Y., Li, W., Tian, Z., Campana, P. E., Li, H., Jin, H., & Yan, J. (2018). Integration of concentrating PVs in anaerobic digestion for biomethane production. Applied Energy, 231, 80–88. doi:10.1016/j.apenergy.2018.09.119

He, S., Qiu, L., Ono, L. K., & Qi, Y. (2020). How far are we from attaining 10-year lifetime for metal halide perovskite solar cells? Materials Science and Engineering: R: Reports, 140, 100545. doi:10.1016/j.mser.2020.100545

Hoffmann, M. M., Duc, P.-F., & Haas, S. (2021). Multi-Vector Simulator (Version v0.5.5, beta release). Zenodo. doi:10.5281/zenodo.4610237

Holmgren, W., Calama-Consulting, Hansen, C., Mikofski, M., Lorenzo, T., Krien, U., ... et al. (2020). pvlib/pvlib-python: v0.8.0 (Version v0.8.0). Zenodo. doi:10.5281/zenodo.4019830

Horowitz, K. A. W., Woodhouse, M., Lee, H., & Smestad, G. P. (2016). A Bottom-Up Cost Analysis of a High Concentration PV Module. doi:10.1063/1.4931548

Hutchins, M. (2020). Oxford PV retakes tandem cell efficiency record.

Kost, C., Mayer, N., Thomsen, J., Hartmann, C., N.and Senkpiel, Philipps, S., Nold, S., ... Schlegl, T. (2013). Levelized cost of electricity renewable energy technologies. Fraunhofer Institute for Solar Energy Systems ISE. Freiburg.

Li, Z., Zhao, Y., Wang, X., Sun, Y., Zhao, Z., Li, Y., ... Chen, Q. (2018). Cost Analysis of Perovskite Tandem Photovoltaics. Joule, 2(8), 1559–1572. doi:10.1016/j.joule.2018.05.001

Lindberg, K. B., Doorman, G., Fischer, D., Korpås, M., Ånestad, A., & Sartori, I. (2016). Methodology for optimal energy system design of Zero Energy Buildings using mixed-integer linear programming. Energy and Buildings, 127, 194–205. doi:10.1016/j.enbuild.2016.05.039

Lisa Anna, Z., Sebastian, N., & Jan Christoph, G. (2020). The Race for Lowest Costs of Electricity Production: Techno-Economic Analysis of Silicon, Perovskite and Tandem Solar Cells. IEEE JOURNAL OF PHOTOVOLTAICS, 10(6), 1632–1641.

Meng, L., You, J., & Yang, Y. (2018). Addressing the stability issue of perovskite solar cells for commercial applications. Nature Communications, 9. doi:10.1038/s41467-018-07255-1

Möller, C., Faulstich, M., & Rosenberger, S. (2019). Urban-rural relations in renewable electric energy supply the case of a German energy region. International Journal of Sustainable Energy Planning and Management, 21, 93–110. doi:10.5278/ijsepm.2019.21.7

Nardin, G., Domínguez, C., Aguilar, Á. F., Anglade, L., Duchemin, M., Schuppisser, D., ... Antón, I. (2020). Industrialization of hybrid Si/IIIV and translucent planar micro-tracking modules. Progress in Photovoltaics: Research and Applications, n/a. doi:10.1002/pip.3387

Nowak, T., Westring, P., & European Heat Pump Association. (2015). European Heat Pump Market and Statistics Report 2015. Retrieved 09/23/2020, from https://www.ehpa.org/fileadmin/red/07._Market_Data/2014/EHPA_European_Heat_Pump_Market_and_Statistics_Report_2015.pdf

oemof developer group. (2016). The oemof demandlib (oemof.demandlib). Zenodo. doi:10.5281/zenodo.438786

on Climate Change (UNFCCC), U. N. F. C. (2016). Paris Agreement. United Nations. Paris, France.

Parliament, E. & Council. (2010). Directive 2010/31/EU on the energy performance of buildings (recast) - 19 May 2010.

Pezzutto, S. (2016). Hotmaps: Heating and Cooling Open Source Tool for Mapping and Planning of Energy Systems. Horizon 2020 Programme of the European Union.

Pless, S. & Torcellini, P. (2010). Net-Zero Energy Buildings: A Classification System Based on Renewable Energy Supply Options. doi:10.2172/983417

pv magazine. (2021). Feed-in tariffs (FITs) in Europe. Retrieved 02/21/2021, from https://www.pv-magazine.com/features/archive/solar-incentives-and-fits/feed-in-tariffs-in-europe/

Renaldi, R., Kiprakis, A., & Friedrich, D. (2017). An optimisation framework for thermal energy storage integration in a residential heat pump heating system. 186, 520–529. doi:10.1016/j.apenergy.2016.02.067

Renno, C., D'Agostino, D., Minichiello, F., Petito, F., & Balen, I. (2019). Performance analysis of a CPV/T-DC integrated system adopted for the energy requirements of a supermarket. Applied Thermal Engineering, 149, 231–248. doi:10.1016/j.applthermaleng.2018.12.007

Renno, C. & Perone, A. (2021). Energy and economic analysis of a point-focus concentrating photovoltaic system when its installation site varies. Frontiers in Energy, 15, 384–395. doi:https://doi.org/10.1007/s11708-020-0717-9

Renno, C. (2014). Optimization of a concentrating photovoltaic thermal (CPV/T) system used for a domestic application. Applied Thermal Engineering, 67(1), 396–408. doi:10.1016/j.applthermaleng.2014.03.026

Ruhnau, O., Hirth, L., & Praktiknjo, A. (2019). Time series of heat demand and heat pump efficiency for energy system modeling. Scientific Data, 6(1), 189. doi:10.1038/s41597-019-0199-y

Schäfer, S. & Brendel, R. (2018). Accurate Calculation of the Absorptance Enhances Efficiency Limit of Crystalline Silicon Solar Cells With Lambertian Light Trapping. IEEE Journal of Photovoltaics, 8, 1156–1158. doi:10.1109/JPHOTOV.2018.2824024

Senatsverwaltung für Wirtschaft, Energie und Betriebe and simuPLAN. (2011). Solarpotentialanalyse Berlin Datendokumentation. Retrieved from https://energieatlas.berlin.de/Energieatlas_Be/Docs/Datendokumentation-Solarkataster_BLN.pdf

Shockley, W. & Queisser, H. J. (1961). Detailed Balance Limit of Efficiency of pn Junction Solar Cells. Jornal of Applied Physics, 32(3), 510–519. doi:10.1063/1.1736034

Sofia, S., Wang, H., Bruno, A., Cruz-Campa, J. L., Buonassisi, T., & Peters, I. (2019). Roadmap for cost-effective, commercially-viable perovskite silicon tandems for the current and future PV market. Sustainable Energy & Fuels, 4. doi:10.1039/C9SE00948E

Sonneveld, P., Swinkels, G., van Tuijl, B., Janssen, H., Campen, J., & Bot, G. (2011). Performance of a concentrated photovoltaic energy system with static linear Fresnel lenses. Solar Energy, 85(3), 432–442. doi:10.1016/j.solener.2010.12.001

Steinbach, I., Haas, S., & Gering, M.-C. (2021). pvcompare: comparing the benefits of different PV technologies in local energy systems in different energy supply scenarios (Version v0.0.3). Zenodo. doi:10.5281/zenodo.4852157

Thygesen, R. & Karlsson, B. (2013). Economic and energy analysis of three solar assisted heat pump systems in near zero energy buildings. Energy and Buildings, 66, 77–87. doi:10.1016/j.enbuild.2013.07.042

Tollin, N. (2016). The role of cities and local authorities following COP21 and the Paris Agreement. Sustainable, 16(1), 43–51.

Vartiainen, E., Masson, G., & Breyer, C. (2015). PV LCOE in Europe 2014-30. doi:10.13140/RG.2.1.4669.5520

Voss, K., Musall, E., Sartori, I., & Lollini, R. (2013). Nearly Zero, Net Zero, and Plus Energy Buildings - Theory, Terminology, Tools, and Examples. In Transition to renewable energy systems (pp. 875–889). Weinheim: Detlef Stolten and Viktor Scherer.

Wiesenfarth, M., Philipps, S. P., Bett, A. W., Horowitz, K., & Kurtz, S. (2017). Current status of concentrator photovoltaic (CPV) technology. Freiburg, Germany.

Williams, C. J. C., Binder, J. O., & Kelm, T. (2012). Demand side management through heat pumps, thermal storage and battery storage to increase local self-consumption and grid compatibility of PV systems. In 2012 3rd IEEE PES Innovative Smart Grid Technologies Europe (ISGT Europe). doi:10.1109/ISGTEurope.2012.6465874

Yang, S., Cannavale, A., Di Carlo, A., Prasad, D., Sproul, A., & Fiorito, F. (2020). Performance assessment of BIPV/T double-skin façade for various climate zones in Australia: Effects on energy consumption. Solar Energy, 199, 377–399. doi:10.1016/j.solener.2020.02.044

Yin, W.-J., Shi, T., & Yan, Y. (2014). Unique Properties of Halide Perovskites as Possible Origins of the Superior Solar Cell Performance. Advanced Materials, 26(27), 4653–4658. doi:10.1002/adma.201306281

Yoshikawa, K., Kawasaki, H., Yoshida, W., Irie, T., Konishi, K., Nakano, K., ... Yamamoto, K. (2017). Silicon heterojunction solar cell with interdigitated back contacts for a photoconversion efficiency over 26%. Nature Energy, 2(5), 17032. doi:10.1038/nenergy.2017.32

Zhao, J., Zheng, X., Deng, Y., Li, T., Shao, Y., Gruverman, A., ... Hwang, I. (2016). Is Cu a Stable Electrode Material in Hybrid Perovskite Solar Cells for a 30-Year Lifetime? Energy Environ. Sci. 9. doi:10.1039/C6EE02980A

A. Annex

A.1. Selection of weather years

Figure 39: **Nine ERA5 weather data years from 2010 to 2018 with electric demand for Berlin, Germany. Three exemplary weather years (2011, 2013, 2016) are chosen to represent a range of different weather years.**

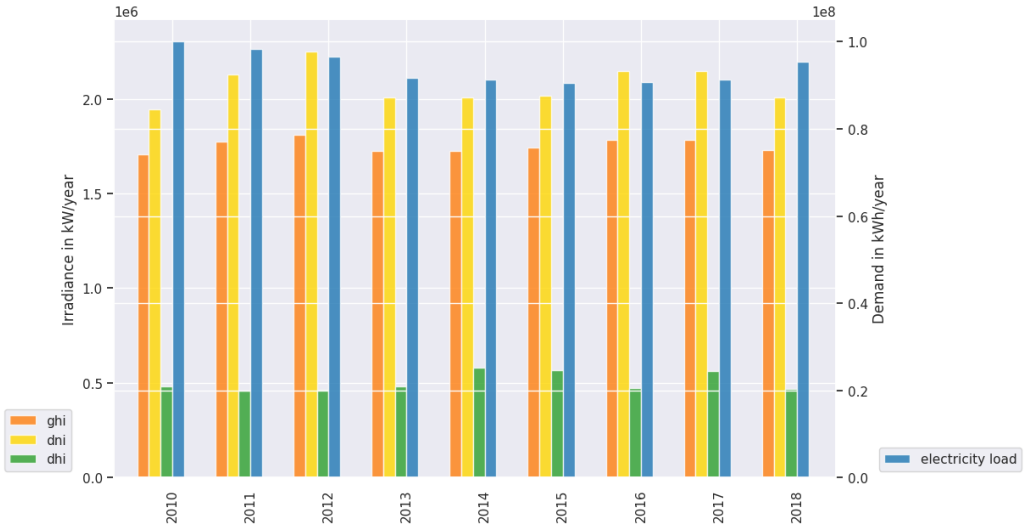

Figure 40: **Nine ERA5 weather data years from 2010 to 2018 with electric demand for Madrid, Spain. Three exemplary weather years (2017, 2013, 2015) are chosen to represent a range of different weather years.**

A.2. Grid parameters

Table 9 lists electricity prices, feed-in tariffs and emission factors of the electricity grid for multiple countries. The electricity prices are obtained from Eurostat, the Statistical Office of the European Union (n.d.-a), most of the feed-in tariffs from pv magazine (2021) and the emission factors from EEA, the European Environment Agency (2021).

Table 9: **Grid parameters (electricity price, feed-in tariff and GHG emissions) for different European countries. If no value is available, the default value is used.**

unit	electricity price EUR/kWh	feed-in tariff EUR/kWh	emission factor $kgCO^2_{eq}$/kWh
Default value	0.18	0.05	0.25
Germany	0.30	0.12	0.34
Greece	0.17	0.12	0.66
Spain	0.22		0.21
France	0.19	0.14	0.05
Italy	0.22		0.25
Latvia	0.14		0.14
Hungary	0.10	0.09	0.25
Poland	0.15		0.79
Romania	0.15		0.29
Finland	0.17	0.11	
United Kingdom	0.22	0.12	0.25

A.3. Scenarios for electricity sector and sector-coupled energy system

The main characteristics of the scenarios for simulating the analysed energy system are displayed in table 10 for the electricity sector and in table 11 for the sector-coupled system. The scenarios are described in sections 2.3.1 and 2.3.2.

Table 10: **Scenarios for simulating the electricity sector of the energy system**

	Sector		Location		Area		PV			Storage	Constraint	Sensitivity analysis	
Name	El	Therm	Berlin	Madrid	Rooftop	Facade	SI	PSI	CPV	Battery		Parameter	(start, stop, step)
Scenario A1-A2	x		1	2	x			x		x		lifetime	(5, 25, 1)
Scenario A3-A6	x		3,5	4,6	x			3,4	5-6	x		specific costs	(500, 1200, 50)
Scenario RefA1-2	x		1	2	x		x			x		–	–
Scenario B1-B7	x		x		x			x		x		lifetime specific costs	(5,25,1) (500, 1100, 100)
Scenario C1-C7	x			x	x			x		x		lifetime specific costs	(5,25,1) (500, 1100, 100)
Scenario D1-D6	x		1-3	4-6	x		1,4	2,5	3,6	x		storeys	(3, 8, 1)
Scenario E1-E6	x		1-3	4-6	x	x	1,4	2,5	3,6	x		storeys	(3, 8, 1)
Scenario F1-F6	x		1-3	4-6	x	x	1,4	2,5	3,6	x	NZE	storeys	(1, 8, 1)
Scenario G1-G6	x		1-3	4-6	x	x	1,4	2,5	3,6	x	maxCap	storeys	(1, 8, 1)
Scenario H1-H12	x		12 cities	in EU	x		x	x	x	x		technology	(si, psi, cpv)
Scenario K1-K12	x		12 cities	in EU	x		x	x	x	x		technology	(si, psi, cpv)

Table 11: **Scenarios for simulating the sector-coupled energy system**

	Sector		Location		Area		PV			Storage		HP		Sensitivity-analysis
Name	El	Therm	Berlin	Madrid	Roof	Fassade	SI	PSI	CPV	Battery	TES	a/a	a/w	Parameter
Scenario RefE1	x		x		x		x			x				
Scenario RefE2	x			x	x		x			x				
Scenario RefG1	x	x	x		x		x			x				
Scenario RefG2	x	x		x	x		x			x				
Scenario A1	x	x	x		x		x			x		x		
Scenario A2	x	x		x	x		x			x		x		
Scenario A3	x	x	x		x		x			x			x	
Scenario A4	x	x		x	x		x			x			x	
Scenario A8	x	x		x	x		x			x		x		storeys
Scenario A14	x	x		x	x	x	x			x		x		storeys
Scenario B1	x	x	x		x		x			x	x		x	
Scenario B2	x	x		x	x		x			x	x		x	
Scenario B5	x	x	x		x		x			x	x		x	storeys
Scenario B9	x	x	x		x	x	x			x	x		x	storeys
Scenario C1	x	x	x		x			x		x	x		x	
Scenario C2	x	x		x	x			x		x		x		
Scenario C3	x	x	x		x				x	x	x		x	
Scenario C4	x	x		x	x				x	x		x		
Scenario C5	x	x	x		x			x		x	x		x	storeys
Scenario C6	x	x		x	x			x		x		x		storeys
Scenario C7	x	x	x		x				x	x	x		x	storeys
Scenario C8	x	x		x	x				x	x		x		storeys
Scenario C9	x	x	x		x	x		x		x	x		x	storeys

Scenario C10	x	x		x	x	x		x	x	x		storeys
Scenario C11	x	x	x		x	x		x	x		x	storeys
Scenario C12	x	x		x	x	x		x	x	x		storeys